



Since January 2020 Elsevier has created a COVID-19 resource centre with free information in English and Mandarin on the novel coronavirus COVID-19. The COVID-19 resource centre is hosted on Elsevier Connect, the company's public news and information website.

Elsevier hereby grants permission to make all its COVID-19-related research that is available on the COVID-19 resource centre - including this research content - immediately available in PubMed Central and other publicly funded repositories, such as the WHO COVID database with rights for unrestricted research re-use and analyses in any form or by any means with acknowledgement of the original source. These permissions are granted for free by Elsevier for as long as the COVID-19 resource centre remains active.

Journal Pre-proof

Rapid discovery and classification of inhibitors of coronavirus infection by pseudovirus screen and amplified luminescence proximity homogeneous assay

Kwiwan Jeong, JuOae Chang, Sun-mi Park, Jinhee Kim, Sangeun Jeon, Dong Hwan Kim, Young-Eui Kim, Joo Chan Lee, Somyoung Im, Yejin Jo, Ji-Young Min, Hanbyeul Lee, Minjoo Yeom, Sang-Hyuk Seok, Da In On, Hyuna Noh, Jun-Won Yun, Jun Won Park, Daesub Song, Je Kyung Seong, Kyung-Chang Kim, Joo-Yeon Lee, Hyun-Ju Park, Seungtaek Kim, Tae-gyu Nam, Wonsik Lee



PII: S0166-3542(22)00242-X

DOI: <https://doi.org/10.1016/j.antiviral.2022.105473>

Reference: AVR 105473

To appear in: *Antiviral Research*

Received Date: 24 August 2022

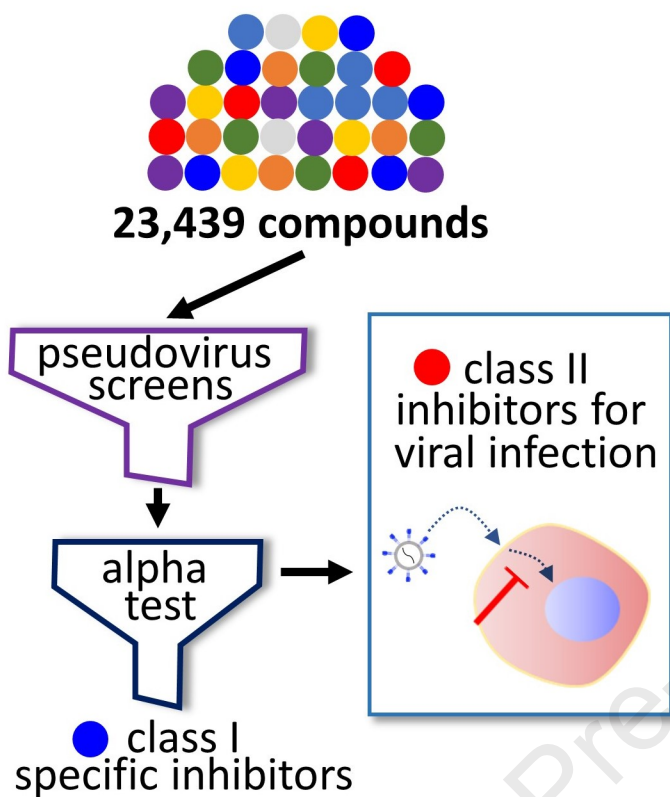
Revised Date: 16 November 2022

Accepted Date: 18 November 2022

Please cite this article as: Jeong, K., Chang, J., Park, S.-m., Kim, J., Jeon, S., Kim, D.H., Kim, Y.-E., Lee, J.C., Im, S., Jo, Y., Min, J.-Y., Lee, H., Yeom, M., Seok, S.-H., On, D.I., Noh, H., Yun, J.-W., Park, J.W., Song, D., Seong, J.K., Kim, K.-C., Lee, J.-Y., Park, H.-J., Kim, S., Nam, T.-g., Lee, W., Rapid discovery and classification of inhibitors of coronavirus infection by pseudovirus screen and amplified luminescence proximity homogeneous assay, *Antiviral Research* (2022), doi: <https://doi.org/10.1016/j.antiviral.2022.105473>.

This is a PDF file of an article that has undergone enhancements after acceptance, such as the addition of a cover page and metadata, and formatting for readability, but it is not yet the definitive version of record. This version will undergo additional copyediting, typesetting and review before it is published in its final form, but we are providing this version to give early visibility of the article. Please note that, during the production process, errors may be discovered which could affect the content, and all legal disclaimers that apply to the journal pertain.

© 2022 Published by Elsevier B.V.



1 **Rapid Discovery and Classification of Inhibitors of Coronavirus Infection**
2 **by Pseudovirus Screen and Amplified Luminescence Proximity**
3 **Homogeneous Assay**

4 Kwiwan Jeong^{1,12,*}, JuOae Chang^{2,12}, Sun-mi Park¹, Jinhee Kim³, Sangeun Jeon³, Dong Hwan
5 Kim⁴, Young-Eui Kim⁵, Joo Chan Lee², Somyoung Im⁴, Yejin Jo⁴, Ji-Young Min³, Hanbyeul
6 Lee⁶, Minjoo Yeom⁶, Sang-Hyuk Seok⁷, Da In On^{8,9}, Hyuna Noh⁹, Jun-Won Yun¹⁰, Jun Won
7 Park⁷, Daesub Song⁶, Je Kyung Seong^{8,9,11}, Kyung-Chang Kim⁵, Joo-Yeon Lee⁵, Hyun-Ju
8 Park^{2,*}, Seungtaek Kim^{3,*}, Tae-gyu Nam^{4,*} and Wonsik Lee^{2,*}

9
10 ¹Gyeonggido Business and Science Accelerator, Suwon, South Korea

11 ²Department of Pharmacy, School of Pharmacy, Sungkyunkwan University, Suwon, South
12 Korea

13 ³Institut Pasteur Korea, Seongnam, South Korea

14 ⁴Department of Pharmacy and Institute of Pharmaceutical Science and Technology, Hanyang
15 University, Ansan, South Korea

16 ⁵Korea Center for Disease Control & Prevention, Cheongju, South Korea

17 ⁶Department of Veterinary Medicine Virology Laboratory, College of Veterinary Medicine and
18 Research Institute for Veterinary Science, Seoul National University, Seoul, South Korea.

19 ⁷Division of Biomedical Convergence, College of Biomedical Science, Kangwon National
20 University, ChunCheon, South Korea

21 ⁸Laboratory of Developmental Biology and Genomics, Research Institute for Veterinary
22 Science, and BK21 Program for Veterinary Science, College of Veterinary Medicine, Seoul
23 National University, Seoul, South Korea

24 ⁹Korea Mouse Phenotyping Center (KMPC), Seoul National University, Seoul, South Korea

25 ¹⁰Laboratory of Veterinary Toxicology, College of Veterinary Medicine, Seoul National
26 University, Seoul, South Korea

27 ¹¹Interdisciplinary Program for Bioinformatics, Program for Cancer Biology and BIO-MAX/N-
28 Bio Institute, Seoul National University, Seoul, South Korea

29 ¹²These authors contributed equally

30

31

32

33 *To whom correspondence should be addressed:

34 Kwiwan Jeong, E-mail: assylum@gbsa.or.kr

35 Hyun-Ju Park, E-mail: hyunju85@skku.edu

36 Tae-gyu Nam, E-mail: tnam@hanyang.ac.kr

37 Seungtaek Kim, E-mail: seungtaek.kim@ip-korea.org

38 Wonsik Lee, E-mail: wonsik.lee@skku.edu

39 **Abstract**

40 To identify potent antiviral compounds, we introduced a high-throughput screen platform that
41 can rapidly classify hit compounds according to their target. In our platform, we performed a
42 compound screen using a lentivirus-based pseudovirus presenting a spike protein of
43 coronavirus, and we evaluated the hit compounds using an amplified luminescence proximity
44 homogeneous assay (alpha) test with purified host receptor protein and the receptor binding
45 domain of the viral spike. With our screen platform, we were able to identify both spike-specific
46 compounds (**class I**) and broad-spectrum antiviral compounds (**class II**). Among the hit
47 compounds, thiosemicarbazide was identified to be selective to the interaction between the
48 viral spike and its host cell receptor, and we further optimized the binding potency of
49 thiosemicarbazide through modification of the pyridine group. Among the **class II** compounds,
50 we found raloxifene and amiodarone to be highly potent against human coronaviruses
51 including Middle East respiratory syndrome coronavirus (MERS-CoV), severe acute
52 respiratory syndrome coronavirus (SARS-CoV), and SARS-CoV-2. In particular, using analogs
53 of the benzothiophene moiety, which is also present in raloxifene, we have identified
54 benzothiophene as a novel structural scaffold for broad-spectrum antivirals. This work
55 highlights the strong utility of our screen platform using a pseudovirus assay and an alpha test
56 for rapid identification of potential antiviral compounds, which can lead to the accelerated
57 development of therapeutics against newly emerging viral infections.

58

59 1. Introduction

60 Human coronaviruses (HCoV) have infected humans and caused diseases that resulted in
61 endemic and recent pandemic crises (Geller et al., 2012; Paules et al., 2020; Song et al.,
62 2019). Since HCoV 229E and OC43 were first reported in the 1960s, for decades they were
63 considered to be the major human-infecting coronaviruses (Cui et al., 2019). However, the
64 emergence of Middle East respiratory syndrome coronavirus (MERS-CoV) in 2012 (Ksiazek
65 et al., 2003; Zaki et al., 2012), which followed the identification of severe acute respiratory
66 syndrome coronavirus (SARS-CoV) in 2002 (Guan et al., 2003; Rota et al., 2003), proved that
67 these pathogenic viruses frequently cross the species border and may pose a significant risk
68 to public health. Recently, COVID-19-causing SARS-CoV-2 (Andersen et al., 2020; Lam et al.,
69 2020; Shang et al., 2020) resulted in over four-million infection cases within six months, and
70 the WHO declared a pandemic (Hu et al., 2021; Huang et al., 2020; Li et al., 2020). Only six
71 months after this declaration, the virus had caused more than 32 million infection cases and
72 posed an enormous threat to public health, putting most nations on hold (Eurosurveillance
73 Editorial, 2020). Despite the substantial effort placed into the development of vaccines
74 (Krammer, 2020; Tregoning et al., 2021), many nations are still putting effort into implementing
75 social distancing or containment policies to prevent further spread of the viral infection due to
76 the continuous appearance of mutant strains. In addition, because there is a possibility of the
77 appearance of infectious mutants of other coronavirus species, there is a pressing and urgent
78 need to develop broad-spectrum antiviral drugs. Today, a few drugs have been licensed for
79 the treatment of COVID-19, but they all display limited efficacy. Therefore, additional antiviral
80 therapeutics applicable to the clinic need to be developed.

81 The entry of coronaviruses into the host cell involves a series of steps, and as an enveloped
82 virus, fusion of the coronavirus membrane with the cellular membrane initiates the early
83 process of entry. This can occur either at the plasma membrane or at a distinct endosomal
84 compartment, which is partially governed by pH-dependent viral fusion machineries (Hartenian
85 et al., 2020). Coronaviruses, including SARS-CoV-2 and MERS-CoV, first attach to the

86 heparan sulfate proteoglycans of the host cell (Hartenian et al., 2020). This initial adherence
87 leads to a bridge interaction with the fusion receptors on the host cell. Coronaviruses employ
88 various cellular fusion receptors: SARS-CoV and SARS-CoV-2 are known to bind to
89 angiotensin-converting enzyme 2 (ACE2) (Li et al., 2005; Li et al., 2003), while MERS-CoV
90 was reported to utilize dipeptidyl peptidase 4 (DPP4) (Raj et al., 2013; Raj et al., 2014). The
91 recognition of host receptors then initiates internalization of the virus *via* various routes
92 (Fuentes-Prior, 2021; Shang et al., 2020), but the most common is the induction of fusion with
93 cellular membrane followed by clathrin-dependent endocytosis (Burkard et al., 2014; Wang et
94 al., 2008; Zhou et al., 2016). The internalization process and fusion factors have been
95 extensively studied, and therefore the early stage of viral infection has been implicated as one
96 of the most favorable drug targets.

97 In our efforts to identify potent inhibitors of coronavirus infection, we have employed a
98 pseudovirus bearing the full-length spike of MERS-CoV for the compound screen of over
99 23,000 small molecules. The resulting 1,200 positive hits were further tested by the amplified
100 luminescence proximity homogeneous assay (alpha) that tested the compound efficacy to
101 prevent the spike-DPP4 interaction. The combination of the two assays allowed rapid
102 classification of the hits into two classes: (1) compounds that prevent binding of the spike to
103 its receptor and (2) compounds that inhibit viral infection independent of spike-receptor
104 interaction. In addition, using our cell-based infection assays, we show that
105 thiosemicarbazides are selectively potent against MERS-CoV infection, while several known
106 drugs including amiodarone and raloxifene have broad-spectrum potency against other
107 coronaviruses including SARS-CoV-2. Importantly, the potency of raloxifene against SARS-
108 CoV-2 was validated by an *in vivo* hamster infection model. In this study, we demonstrate that
109 the pseudovirus-based screen and alpha test combined with other *in vitro* and *in vivo* assays
110 are useful for the rapid identification of efficacy measures and mechanism of action of
111 compounds.

112

113 2. Materials and Methods

114 2.1. Cell line and virus maintenance

115 Lenti-X™ 293T cells (Clontech, Mountain View, CA) were cultivated in Dulbecco's Modified
116 Eagle's Medium (DMEM; Sigma-Aldrich, St. Louis, MO) supplemented with 4.5 g/L glucose, 4
117 mM L-glutamine, 3.7 g/L NaHCO₃, 10% fetal bovine serum (FBS; Gibco, Billings, MT), 1 mM
118 sodium pyruvate (Sigma-Aldrich), and 1% penicillin/streptomycin (Sigma-Aldrich). Huh-7 cells
119 (KCLB, Seoul, South Korea) were cultured in Roswell Park Memorial Institute (RPMI-1640;
120 Gibco) medium supplemented with 10% FBS and 1% penicillin/streptomycin. Vero cells (ATCC,
121 Manassas, VA) were cultured in Opti-PRO™ SFM (Gibco) supplemented with 4 mM L-
122 glutamine and 1× Antibiotic-Antimycotic (Gibco). Vero E6 cells were cultured in DMEM
123 (Corning Incorporated, Corning, NY) containing 5% FBS. MRC-5 cells were cultured in Eagle's
124 Minimum Essential Medium (EMEM, Gibco) supplemented with 10% FBS and 1%
125 penicillin/streptomycin. All mammalian cells were maintained at 37°C in a humidified 5% CO₂
126 incubator unless otherwise noted. Serum-free media (SFM)-adapted *Spodoptera frugiperda* 9
127 (Sf9) cells (Thermo Fisher Scientific, Waltham, MA) were cultured in Sf-900™ III SFM medium
128 at 27°C with continuous agitation. Patient-derived MERS-CoV (passage 4, MERS-
129 CoV/KOR/KNIH/002_05_2015; GenBank: KT029139.1) was obtained from the Korea Centers
130 for Disease Control and Prevention. SARS-CoV (HKU39849) was obtained from the University
131 of Hong Kong-Pasteur Research Pole. Human coronavirus 229E (HCoV-229E) and human
132 coronavirus OC43 (HCoV-OC43) were obtained from ATCC.

133

134 2.2. Chemical compounds and antibodies

135 The chemical library used for high-throughput screen consists of 978 drugs from the FDA-
136 approved drug library (Selleckchem, Houston, TX) and 1280 compounds from the Library of
137 Pharmacologically Active Compounds (LOPAC®¹²⁸⁰; Sigma-Aldrich). All stock compounds
138 were at 10 mM in DMSO. Amiodarone, raloxifene, and chloroquine were purchased from
139 Sigma-Aldrich. The analogs were synthesized as described in the **Supplementary**

140 **Information.** The spike antibody was purchased from Sino Biological (R723; Beijing, China).
141 Analogs of compound **2** were purchased as described in **Fig. S13**.

142

143 **2.3. Pseudovirus preparation**

144 The pseudovirus was produced as previously described (Zhao et al., 2013). A spike expression
145 vector (pCMV3-Flag-CD5-Spike) was constructed by inserting the CD5 signal sequence
146 upstream of the spike coding sequence of the pCMV3-Flag-Spike (betacoronavirus 2c EMC
147 2012) vector (VG40069-CF; Sino Biological), after which 4.5×10^6 Lenti-X™ 293T cells were
148 co-transfected with 10 µg of a luciferase expression vector (pLenti-CMV-puro-luc; Addgene,
149 Water Town, MA) (Campeau et al., 2009), 10 µg of a packaging vector (pCMVΔ8.2-dvpr;
150 Addgene) (Stewart et al., 2003), and 600 ng of pCMV3-Flag-CD5-Spike in a 100 cm² cell
151 culture dish using the calcium phosphate transfection method (Invitrogen, Waltham, MA). After
152 48-hour incubation, the virus-containing supernatant was harvested and concentrated using
153 the Retro-X™ concentrator (Clontech) followed by titration using the Lenti-X™ p24 Rapid Titer
154 kit (Clontech). As a positive control, a pseudovirus of vesicular stomatitis virus (VSV) was
155 generated using pCMV-VSV-G (Sino Biological) as an envelope vector; and as a negative
156 control, a pseudovirus of negative control vector (NCV) was generated using pCMV3FLAG-
157 NCV (Sino Biological) as an envelope vector.

158

159 **2.4. Pseudovirus infection assay**

160 Huh-7 cells were plated in white 384-well plates at a density of 4×10^4 cells/well. After overnight
161 incubation, compounds at a final concentration of 10 µM and pseudovirus at 5×10^3 IFU were
162 added in sequence. Following a 72-hour incubation, 20 µl of Bright-Glo® reagent (Promega,
163 Madison, WI) was dispensed into each well, and the relative luminescence unit (RLU) was
164 measured using an EnVision® multilabel plate reader (PerkinElmer, Waltham, MA). The
165 inhibition of pseudovirus-derived luminescence was presented as % inhibition, which was
166 calculated using the following equation: $([RLU_{pc} - RLU_{sample}] / [RLU_{pc} - RLU_{nc}] \times 100)$, where

167 pc and nc respectively indicate pseudovirus-infected positive control and mock-infected
168 negative control. The cytotoxicity of compounds used in the screen was assessed using the
169 CellTiter-Glo[®] reagent (Promega). Cytotoxicity was also presented in the manner described
170 above, with pc meaning DMSO treatment and nc meaning media without cells. Activity of the
171 hit compounds were examined by dose-response curve (DRC) analysis. For the high-
172 throughput screening and DRC analyses, we fixed the viral titer and cell number to 5 IFU and
173 4×10^3 Huh-7 cells, respectively, in a 384-well plate, which resulted in a robust Z' score of ~0.6.
174 From the DRC analyses, 50% effective concentrations (EC_{50}) and 50% cytotoxic
175 concentrations (CC_{50}) were calculated using the non-linear regression formula of GraphPad
176 Prism 6 software (GraphPad Software, La Jolla, CA).

177

178 **2.5. Purification of hDPP4 and spike RBD proteins**

179 For the expression of MERS-CoV spike RBD, we constructed a pFastbac-HBM-RBD(367~606)
180 vector by cloning an RBD gene (residues 367~606) amplified from the pCMV3-Flag-Spike
181 vector using the Bac-to-Bac[®] HBM TOPO[®] cloning kit (Invitrogen). To introduce an N-
182 terminal GP67 signal sequence in place of HBM and to insert C-terminal Strep-tag[®]II, we
183 constructed a pFastbac-GP67-RBD(367~606)-Strep-tag[®]II vector by cloning a codon-
184 optimized 906 bp gene encoding GP67-RBD(367~606)-Strep-tag[®]II (GenBank: AKN11075.1)
185 into the pFastbac-HBM-RBD(367~606) vector using BamHI/XhoI restriction sites. For the
186 expression of hDPP4 with a C-terminal hexa-histidine tag, we constructed a plasmid,
187 pFastbac-HBM-hDPP4(39~766), by cloning codon-optimized hDPP4 (residues 39~766) using
188 the Bac-to-Bac[®] HBM TOPO[®] cloning kit (Invitrogen). The pFastbac-GP67-RBD(367~606)-
189 Strep-tag[®]II vector and the pFastbac-HBM-hDPP4(39~766) were each transformed into MAX
190 Efficiency[™] DH10Bac[™] competent cells (Invitrogen), at which point the recombinant bacmid
191 DNAs were extracted and transfected into Sf9 cells using Cellfectin[™] reagent (Invitrogen).
192 After incubation for 7 days, P1 viral stocks were harvested, reinoculated, and further amplified.

193 The resulting P2 viral stocks were titrated with the plaque assay, and a high titer ($0.5\sim 1\times 10^9$
194 pfu) was inoculated in 1 L of Sf9 cells. Supernatant containing the target protein was harvested
195 3 days after inoculation. The supernatant containing RBD was equilibrated by the addition of
196 100 mL of 10× buffer W (1 M Tris-Cl, pH 8.0, 1.5 M NaCl, 10 mM EDTA), and endogenous
197 biotin was blocked by incubation with 2.4 mL of BioLock Biotin blocking solution (IBA
198 Lifesciences, Göttingen, Germany). Debris was filtered out using a Nalgene™ Rapid-Flow™
199 filter (Thermo Scientific). Strep-tag®II (STII)-tagged RBD was purified using Strep-Tactin®
200 Sepharose beads (IBA Lifesciences) according to the manufacturer's instructions. The
201 supernatant containing hDPP4 was filtered with the same filter mentioned earlier, and it was
202 then consecutively purified with affinity chromatography using Ni sepharose® 6 Fast Flow
203 beads (GE Healthcare, Chicago, IL) and ion exchange chromatography using SP sepharose®
204 Fast Flow beads (GE Healthcare). Each protein eluate was concentrated using Vivaspin
205 centrifugal concentrators (Satorious, Göttingen, Germany) and buffer-exchanged in a dialysis
206 buffer (PBS, pH 7.4, 10% glycerol) for 12 hours at 4°C.

207

208 **2.6. Alpha test**

209 In the alpha test, a photosensitizer in the "Donor" bead converts ambient oxygen to a more
210 excited singlet state. The singlet state oxygen molecules diffuse across to react with a thioxene
211 derivative in an acceptor bead, generating chemiluminescence at 370 nm, which further
212 activates the fluorophores to emit light at 520-620 nm. Before screening, we excluded false
213 positives by separately testing the compounds for their ability to quench singlet oxygen or
214 emission light using the AlphaScreen® TrueHits kit and optimized the concentrations of
215 proteins and beads. The optimized assay was performed in assay buffer containing 1× PBS,
216 pH 7.4, 0.01% Tween 20, and 0.1% BSA in a white 384-well OptiPlate® (PerkinElmer) at 25°C.
217 For the reaction, compounds (20 µM) were first incubated with recombinant hDPP4 protein
218 (25 nM) and then with RBD protein (100 nM) for 15 minutes each, after which 5 µg/mL of each

219 of Strep-Tactin[®] AlphaLISA[®] Acceptor bead (PerkinElmer) and Nickel Chelate Alpha Donor
220 bead (PerkinElmer) were added. The Alpha signals were measured using an EnVision[®]
221 multilabel plate reader (PerkinElmer) after 1-hour incubation in the dark. The activity of the hit
222 compounds was determined by the DRC experiments, and the 50% inhibitory concentrations
223 (IC₅₀) values were calculated using the GraphPad Prism 6 software (GraphPad Software).

224

225 **2.7. Pull-down assay of hDPP4 and spike RBD**

226 For the pull-down assay, purified hDPP4 and RBD proteins were incubated at 4°C for 1 hour,
227 followed by incubation with Ni Sepharose 6 Fast Flow beads for 2 hours. After being washed
228 three times with the assay buffer containing 1× PBS, pH 7.4, 0.01% Tween 20, and 0.1% BSA,
229 the assay was performed in duplicate, out of which one reaction was analyzed by SDS-PAGE
230 and Coomassie Blue staining and the other by immunoblot using the Strep-Tactin[®]-HRP
231 conjugated antibody (IBA Lifesciences).

232

233 **2.8. ELISA**

234 An hDPP4 protein (5 µg/mL) was immobilized on a Ni-coated 96-well plate (Thermo Scientific).
235 After 1-hour incubation and washing, serially diluted compounds and RBD were added to the
236 plate. Following another 1-hour incubation and washing, Strep-Tactin[®]-HRP conjugate (IBA
237 Lifesciences) was added, and the reaction proceeded for an hour. After being washed three
238 times, 50 µl of 1-Step[™] ultra TMB-ELISA (Thermo Scientific) was added, and the chromogenic
239 reaction continued until the appropriate color was developed. Upon termination of reaction by
240 addition of sulfuric acid, absorbance was measured at 450 nm using a FlexStation[®] 3 multi-
241 mode microplate reader (Molecular devices, San Jose, CA). The IC₅₀ values of the test
242 compounds were calculated using the GraphPad Prism 6 software (GraphPad Software).

243

244 **2.9. *In silico* docking**

245 To understand the inhibition mechanism of compound **1**, docking analysis of hit compounds

246 was performed using Schrodinger's Maestro 11.6 software. First, structures of the hits were
247 sketched using a 2D sketch module, and a maximum of 32 tautomers that retained specified
248 chiralities and possible ionization states at pH 7.0 were generated for each structure. Then,
249 energy-minimization was conducted under the OPLS4e force field to obtain a stable
250 conformation. Prior to docking, the X-ray co-crystal structure of MERS-CoV RBD in complex
251 with DPP4 (PDB: 4L72) and the apo-structure of MERS-CoV RBD (PDB: 4L3N) were retrieved
252 from the Protein Data Bank (www.rcsb.org). To optimize the structures of the proteins, the
253 assignment of bond orders, removal of original hydrogens, generation of het states, and
254 removal of duplicated side chains and water molecules were performed sequentially. A brief
255 minimization was conducted in the OPLS3e force field using the default option. Several
256 docking sites of protein were defined using a grid generation module by picking key residues
257 and adjacent residues in the hDPP4 binding region of MERS-CoV RBD. To perform
258 extra/precision Glide docking, XP docking was selected, and at least 10 poses per compounds
259 were generated. The binding affinity of each of the docking poses of the ligand was calculated
260 using the Glide docking score function. The most plausible binding mode of compound **1** was
261 selected based on 3D docking poses, glide docking score, and visual inspection of the
262 interactions between the ligand and key residues.

263

264 **2.10. Electrostatic complementarity analysis**

265 Electrostatic complementarity analysis was conducted using Cresset's Flare 3.0.0 software
266 (Cheeseright et al., 2006). The best docking poses of compound **1** and **1h** bound to the target
267 protein (MERS-CoV spike RBD) were exported as SDF files and reloaded into the Flare
268 program. The electrostatic complementary surface and score of each ligand were calculated
269 in terms of the XED molecular mechanics force field using a default setting.

270

271 **2.11. Cellular cholesterol measurement**

272 Total cholesterol levels were measured using the Cholesterol Ester-Glo™ assay (Promega)

273 according to the manufacturer's instructions. Briefly, A549 and Huh-7 cells were seeded in
 274 white bottom 96-well plates at a density of 1×10^4 cells and incubated overnight. The cells were
 275 then treated with 10 μ M raloxifene and incubated for 12 hours, after which, a reagent
 276 containing cholesterol dehydrogenase, which luminesces under the presence of free
 277 cholesterol, is added. The luminescence intensity was measured using the Synergy HTX multi-
 278 mode plate reader (BioTek, Winooski, VT).

279

280 **2.12. qRT-PCR of genes involved in the cholesterol pathway**

281 A549 cells were seeded in 6-well plates at a density of 1×10^6 cells/well and incubated
 282 overnight. The cells were then treated with 10 and 50 μ M raloxifene and incubated for 12 hours,
 283 after which RNA was isolated using Ambion TRIzol reagent (Thermo Scientific) according to
 284 the manufacturer's instructions. RNA (5 μ g) was reversely transcribed into cDNA using RNA
 285 to cDNA ecoDry Premix (Takara, Kusatsu, Japan), which was further used for real-time
 286 polymerase chain reaction using SYBR green 2 \times Master Mix (Elpis, Daejeon, South Korea).
 287 The primers used for the analysis are as follows:

Target	Sequence	Source
MSR1	F: TGCACAAGGCAGCTCACTTTGG R: GTGCAAGTGACTCCAGCATCTTC	(Yang et al., 2020)
FASN	F: GTTCACGGACATGGAGCAC R: GTGGCTCTTGATGATCAGGTC	(Che et al., 2020)
Sqle	F: GTTCGCCCTCTTCTCGGATATT R: GGTTCCTTTTCTGCGCCTCCT	(Che et al., 2020)
CH25H	F: GCTGGCAACGCAGTATATGA R: ACGGAAAGCCAGATGTTGAC	(Che et al., 2020)
Actin	F: TCATGAAGTGTGACGTGGACATC R: CAGGAGGAGCAATGATCTTGATCT	(Che et al., 2020)

288

289 **2.13. Image-based immunohistochemistry infection assay**

290 Vero cells were seeded at 1.2×10^4 cells per well in black 384-well μ Clear plates (Greiner bio-
 291 one, Kremsmünster, Austria) 24 hours prior to experimentation. Test compounds were added
 292 to each well at the desired concentrations prior to virus infection. The DMSO concentration
 293 was kept at 0.5% or below. For infection with MERS-CoV at an MOI of 0.0625, plates were

294 transferred into the BSL-3 containment laboratory. Infection was arrested at 24 hours post-
295 infection by adding 4% PFA followed by immunofluorescence staining. MERS-CoV infection
296 was detected using a rabbit anti-MERS-CoV spike antibody (Sino Biological), and cell viability
297 was evaluated with Hoechst 33342 stain (Jeon et al., 2020). The same procedures were
298 performed for SARS-CoV . Data were acquired by taking images at 20× magnification using
299 an Operetta high-content imaging system (Perkin Elmer), and the images were analyzed by
300 an in-house developed software, Image Mining 3.0 (IM 3.0) plug-in. To validate the assay,
301 DRC experiments with two compounds with known antiviral activities against MERS-CoV—
302 chloroquine diphosphate and lopinavir—were performed (de Wilde et al., 2014). Test
303 compounds were evaluated by duplicate, 10-point DRC at a concentration range of 50~0.0977
304 μM . Percent inhibition (PI) was normalized as follows: $\text{PI} = [1 - (\text{IN}_{\text{test}} - \mu\text{IN}_{\text{mock}}) / (\mu\text{IN}_{\text{vehicle}} - \mu\text{IN}_{\text{mock}})] \times 100$, where IN_{test} is percent infection of test compound, $\mu\text{IN}_{\text{mock}}$ is average
305 of mock, and $\mu\text{IN}_{\text{vehicle}}$ is average of infection control. Percent viability (PV) was calculated
306 as follows: $\text{PV} = (\text{CN}_{\text{test}} / \mu\text{CN}_{\text{mock}}) \times 100\%$, where CN_{test} and $\mu\text{CN}_{\text{mock}}$ are the cell
307 numbers in the treatment groups and average cell number in the mock group, respectively.
308 After normalization, the EC_{50} and CC_{50} were calculated with the nonlinear regression of
309 GraphPad Prism software. Selective index (SI) was calculated by dividing CC_{50} with EC_{50} (Ko
310 et al., 2021).

312

313 **2.14. Time-of-addition assay**

314 Vero cells seeded in a 96-well microplate (2×10^4 cells/well) were incubated for 24 h prior to
315 compound treatment and virus inoculation. Compounds were treated at 1 h intervals from -1
316 h pre-infection to 6 h post-infection. At the 0 h time point, cells were inoculated with the virus
317 at an MOI of 5 and incubated at 4°C for 1 h to allow the virus to bind to the cell surface for
318 synchronization. Subsequently, the cells were washed to remove unbound viruses and the
319 temperature was shifted to 37°C to promote viral uptake into the cells. The cells were cultured
320 with a drug-containing medium until the end of the experiment and cells were fixed at 7 h post-

321 infection and analyzed by immunofluorescence assay as previously described (Daelemans et
 322 al., 2011; Jeong et al., 2022; Shin et al., 2022). The images were acquired and analyzed as
 323 mentioned in the **Image-based immunohistochemistry infection assay** section.

324

325 **2.15. qRT-PCR of viral titer**

326 For analysis of the viral titer of MERS-CoV, Vero cells were seeded at 3×10^5 cells per well in
 327 24-well plates 24 hours prior to experimentation. The test compounds were added at the final
 328 concentrations of 1, 3, 10, and 30 μM to each well before MERS-CoV infection; the DMSO
 329 concentration was kept at 0.5% or lower. The plates were moved to the BSL-3 containment
 330 laboratory prior to inoculation with MERS-CoV at an MOI of 0.0625. After 24 hours, the cells
 331 were washed with PBS and lysed in RLT buffer of the RNeasy® mini Kit (QIAGEN, Valencia,
 332 CA) supplemented with 1% β -mercaptoethanol (Sigma-Aldrich). The cell lysates were moved
 333 to the BSL-2 containment laboratory, where total RNA was isolated using the kit and eluted in
 334 50 μl of DEPC-treated water. MERS-CoV viral RNA was quantified through multiplex real-time
 335 reverse-transcription polymerase chain reaction (RT-PCR) using the TOPscript™ One-step
 336 RT-PCR DryMIX kit (Enzynomics, Daejeon, South Korea). The primers used were as follows:

Target	Sequence	Source
upE of MERS-CoV	F: GCAACGCGCGATTTCAGTT R: GCCTCTACACGGGACCCATA	(Corman et al., 2012)
upE probe	6-carboxyfluorescein [FAM]- CTCTTCACATAATCGCCCCGAGCTCG-6- carboxy-N,N,N,N'-tetramethylrhodamine [TAMRA]	(Corman et al., 2012)
GAPDH	F: GAAGGTGAAGGTTCGGAGTCAAC R: CAGAGTTAAAAGCAGCCCTGGT	(Corman et al., 2012)
GAPDH probe	6-carboxy-4',5'-dichloro-2',7'- dimethoxyfluorescein [JOE]- TTTGGTCGTATTGGGCGCT-6-TAMRA	(Corman et al., 2012)

337

338 For analysis of the viral titer of HCoV-229E and HCoV-OC43, total RNA was isolated from
 339 virus- or mock-infected MRC-5 cells using the TRIzol reagent (Invitrogen) at the indicated time
 340 points. cDNA synthesis and RT-PCR were conducted using the 2× One Step RT-PCR
 341 MasterMix with SYBR Green (MGmed, Seoul, South Korea) according to the manufacturer's

342 instructions. The sequences of target genes and primers used are as follows:

Target	Sequence	Source
HCoV-229E	F: CGCAAGAATTCAGAACCAGAG R: GGCAGTCAGGTTCTTCAACAA	(Niu et al., 2016)
HCoV-OC43	F: ACTCAAATGAATTTGAAATATGC R: TCACACTTAGGATAATCCCA	(Niu et al., 2016)
GAPDH	F: GTCGGAGTCAACGGATT R: AAGCTTCCC GTTCTCAG	(Niu et al., 2016)

343

344 **2.16. Cytopathic effect (CPE) assay**

345 MRC-5 cells were seeded at 2×10^3 cells per well in a white opaque 384-well plate. After 24
 346 hours of incubation, serially diluted compounds were treated 2 hours before HCoV-229E
 347 infection at an MOI of 5. Following an additional 48 hours of incubation, cell viability was
 348 measured 20 minutes after adding CellTiter-Glo reagent containing 1% TX-100 using an
 349 EnVision[®] multilabel plate reader. EC₅₀ was then calculated with the non-linear regression
 350 formula of GraphPad Prism 6 software.

351

352 **2.17. SARS-CoV-2 infection assay**

353 Vero cells were seeded at 2×10^3 cells per well in a white opaque 384-well plate. After 24 hours
 354 of incubation, the cells were treated with serially diluted compounds 2 hours before SARS-
 355 CoV-2 infection at an MOI of 0.0125. Following 48 hours incubation, cell viability was
 356 measured by adding the CellTiter-Glo reagent containing 1% TX-100 and by measuring the
 357 luminescence with a plate reader after 20 minutes. EC₅₀ was calculated using the non-linear
 358 regression formula of GraphPad Prism 6 software.

359

360 **2.18. Hamster experiment**

361 ***Biosafety and ethics***

362 All experimental procedures were performed in the BSL-3 facility of the Korea Zoonosis
 363 Research Institute at Jeonbuk National University. All work using live SARS-CoV-2 was
 364 approved by the Institutional Biosafety Committee of Jeonbuk National University. All

365 experimental procedures involving animals were approved by the Institutional Animal Care
366 and Use Committee of Jeonbuk National University (JBNU-2020-63) and conducted in
367 accordance with the institutional guidelines.

368

369 ***Production of virus***

370 SARS-CoV-2 virus (NCCP 43326) was provided by the Korea Center for Disease Control and
371 Prevention (Cheongju, South Korea); it was propagated in African green monkey kidney
372 epithelial (Vero E6) cells.

373

374 ***Animals***

375 Male Syrian hamsters (*Mesocricetus auratus*) aged 13 to 14 weeks old were purchased from
376 SLC Inc. (Shizuoka, Japan). Hamsters were anaesthetized with isoflurane and intranasally
377 inoculated with $1 \times 10^{5.5}$ TCID₅₀ of SARS-CoV-2 in 50 μ l DMEM. Two experimental groups of
378 hamsters (n=12/group) inoculated with virus were treated orally with either 12 mg/kg (low dose)
379 or 36 mg/kg (high dose) of raloxifene, respectively. Drug treatment was initiated 4 hours after
380 infection, and the drug was administered once daily for 5 days. Hamsters inoculated with virus
381 (untreated) and PBS were respectively used as the positive and negative control (n=6/group).
382 The hamsters were monitored daily for body weight, mortality, and clinical signs. At two days
383 post infection, animals (n=6 per experimental group and n=3 for the control group) were
384 euthanized for necropsies, and tissue samples were collected for further analysis. Tissue
385 samples were placed into tissue homogenizing CK14 tubes (Precellys, Bertin Technologies,
386 Montigny-le-Bretonneux, France) prefilled with ceramic beads and DMEM, then homogenized
387 using a Bead blaster 24 (Benchmark Scientific, Sayreville, NJ). Nasal turbinate and right lung
388 lobes were used to determine the viral titer (TCID₅₀) and viral RNA load (qRT-PCR). The other
389 lung lobes were fixed in 10% neutral buffered formalin (NBF) for histopathological examination
390 (Klopfleisch, 2013).

391

392 Viral titration and measurement of viral RNA load

393 Vero E6 cells were plated the day before infection into 96-well plates at 2×10^4 cells/well. After
394 centrifugation of the homogenized tissue samples, the supernatants were inoculated into Vero
395 E6 cells at 10-fold serial dilutions. The cells were monitored for 3 days for recording of CPE
396 for three days. The TCID₅₀ was calculated using the Spearman & Kärber algorithm. Viral RNA
397 was extracted from the supernatants of homogenized tissue using the QIAamp viral RNA Mini
398 Kit (Qiagen) according to the manufacturer's protocol. Quantitative real-time PCR (qRT-PCR)
399 was performed on a LightCycler96 platform (Roche, Basel, Swiss) with commercial one-step
400 real-time PCR kits for SARS-CoV-2 (Allplex 2019-nCoV Assay kit, Seegene, Seoul, South
401 Korea). The thermal profile consisted of 1 cycle for 20 min at 50°C, 1 cycle for 15 min at 95°C,
402 and 45 cycles of 15 s at 94°C and 30 s at 58°C. The results were analyzed using 2019-nCoV
403 viewer from Seegene Inc. according to the manufacturer's instructions.

404

405 2.19. Statistical analysis

406 Statistical analyses between multiple experimental groups were conducted by one-way
407 ANOVA followed by Dunnett's multiple comparison tests. The results were expressed in the
408 form of mean \pm standard error of mean (SEM). Differences between groups were considered
409 significant for values of $p < 0.05$. Statistical analyses were conducted using Prism 6 software
410 (GraphPad Software).

411

412 3. Results

413 3.1. Inhibitors of MERS-CoV infection were identified through a phenotypic high- 414 throughput screen

415 We sought to establish a cell-based phenotypic high-throughput screen (HTS) platform to
416 identify compounds that may inhibit the viral infection using MERS-CoV as a model
417 coronavirus. We generated a chimeric pseudovirus presenting the full-length spike protein of
418 the MERS-CoV as previously demonstrated (Zhao et al., 2013). Then, in a 384-well plate
419 format, Huh-7 cells were infected with the pseudovirus, and the infected cells constitutively
420 expressed luciferase over a two-day period (**Fig. 1a** and **S1a**). To validate the pseudovirus
421 infection, we preincubated the Huh-7 cells with the heptad repeat 2 peptide (HR2P), which is
422 a known inhibitor of MERS-CoV infection (Bosch et al., 2004; Liu et al., 2009), and we found
423 that the luciferase signal from the infected Huh-7 cells was reduced in a dose-dependent
424 manner (**Fig. S1b**). This indicates that the luminescence signal from the infected cells can
425 serve as a marker of pseudovirus infection.

426 Using our pseudovirus-based screen platform, we tested 23,439 small molecules from either
427 the FDA-approved compound library or pharmacologically active compound library at the
428 single concentration of 10 μ M. Hit compounds were identified by their ability to reduce the
429 luciferase signal (**Fig. S1c**). In parallel, we performed a cytotoxicity screen in the absence of
430 the pseudovirus at a final compound concentration of 20 μ M, which allowed us to exclude
431 comparably cytotoxic compounds (>20% cell death) (**Fig. S1d**). From the screen, we identified
432 1,126 hits that displayed low cytotoxicity and high inhibition in the range of 70-100% compared
433 to the control (**Fig. 1c, S1c, and S1d**). The average of the calculated Z' factors for 80 screening
434 plates was \sim 0.62, indicating that the screen was robust (**Fig. S1e**). Since our pseudovirus is
435 incapable of replicating and generating newly made viral progenies inside the infected cells,
436 we reasoned that the hits identified through the pseudovirus screen would be those capable
437 of preventing the early stages rather than the later stages of viral infection. Importantly, this
438 allows us to narrow down the potential antiviral targets of hit compounds and thus aid in the

439 rapid identification of their molecular mechanism of action.

440

441 **3.2. Hits were screened for their ability to inhibit hDPP4 and spike interaction by alpha**

442 We sought to further confirm whether our hit compounds inhibit interaction between hDPP4
443 and the spike of MERS-CoV. To this end, we set up an *in vitro* protein-based alpha assay
444 (Schorpp et al., 2014; Ullman et al., 1994), as described in **Fig. 1b**. Specifically, due to the
445 complexity and insolubility of the full-length spike protein, we used the 28-kDa RBD of the S1
446 of the MERS-CoV spike (Park et al., 2019; Xia et al., 2014) to attach to phthalocyanine, a
447 singlet oxygen donor, and coupled the hDPP4 to a thioxene derivative as a singlet oxygen
448 acceptor. Since the alpha test allowed us to directly monitor the interaction between the RBD
449 and hDPP4, we reasoned that this alpha test could classify our primary hit compounds into a
450 class of compounds specifically targeting the spike-receptor interaction (**class I**) and a class
451 of compounds that potentially achieve their antiviral activity through inhibition independent of
452 the binding between the spike and its receptor (**class II**).

453 Because we used the RBD of the S1 protein, and not full-length S1, we first determined
454 whether the purified RBD interacts with the purified hDPP4 in our assay conditions (Li, 2016).
455 As shown in **Fig. S2a**, we were able to capture the hDPP4 protein using the purified RBD
456 protein in our pull-down assay, suggesting that the purified RBD protein retains the ability to
457 interact with hDPP4 in the given conditions. We were able to further optimize the alpha
458 condition by testing combinations of various concentrations of hDPP4 and RBD (**Fig. S2b**),
459 and when tested with an antibody (R723) of the viral spike, we found that the alpha signal was
460 reduced in a dose-dependent manner (**Fig. S2c**), which validates our alpha conditions.
461 Subsequently, we examined 1,126 primary hits obtained from the pseudovirus screen and
462 found 188 out of 1,126 compounds were validated for antagonistic activity specifically on the
463 interaction between the RBD and hDPP4, in the range of >40% inhibition relative to the control
464 (**Fig. 1c**). We note that this group (**class I**) of compounds displays significance as inhibitors of
465 spike-receptor interaction, and our results demonstrate that the combination of the

466 pseudovirus screen and the *in vitro* alpha test can be used to rapidly identify the mechanisms
467 of action of inhibitors by specifying their targets.

468

469 **3.3. Thiosemicarbazide (class I) inhibits MERS-CoV infection by antagonizing the** 470 **binding of the spike to the hDPP4**

471 Among the 188 **class I** inhibitors, a thiosemicarbazide compound showed outstanding potency,
472 so we further tested its analogs (**Fig. 1d** and **2a**). As shown in **Fig. 2b**, compound **J1** showed
473 potency in both the pseudovirus assay (EC_{50} , 1.1 μ M) and alpha test (IC_{50} , 6.28 μ M). To
474 conduct structure activity relationship (SAR) studies, we synthesized a total of 25
475 thiosemicarbazide analogs by modifying the compound **J1** (**Fig. 2a**). The results of the SAR
476 studies revealed that the 2-pyridine group on the left portion of the molecule is more crucial
477 for activity than the linker region or phenyl group on the right side. We found that the efficacy
478 of thiosemicarbazide was abolished or reduced when we replaced the 2-pyridine moiety with
479 other groups, including 6-fluoro and 6-hydroxy pyridine (**1b-3** and **1b-1**). However, when we
480 replaced the *p*-chlorophenyl on the right side with *p*-trifluoromethylphenyl (**1g-8**), 6-
481 methoxypyridine (**1j**), or 4-methylcyclohexyl (**1g-5**) groups, their potency in the alpha test was
482 highly improved (**1g-8**, IC_{50} =2.92 μ M; **1j**, IC_{50} =0.85 μ M; **1g-5**, IC_{50} =0.85 μ M) (**Fig. 2b**). As
483 expected, when we modified the thiosemicarbazide backbone, potency was completely
484 abolished (**1d** and **1e**). The SAR analysis suggests that the pyridine moiety is a potential
485 pharmacophore through which thiosemicarbazide analogs may bind to the target. We also
486 found that several modifications of the pyridine group such as in 4-methylcyclohexyl (**1g-5**)
487 resulted in a significantly increased cytotoxicity (**Fig. 2b**). Therefore, we excluded the toxic
488 analogs including **1g-5** (CC_{50} , 18.81 μ M), and further examined the selected compounds using
489 ELISA designed to capture RBD with immobilized hDPP4 (**Fig. 2c**). We found that **1** and **1g-**
490 **8** were validated while **1j** showed a lower inhibitory effect (**Fig. 2d-2f**). Since we used the RBD,
491 which is a part of S1 of MERS-CoV, in the alpha test, we retested **1g-8** and **1j** with a
492 pseudovirus expressing the full-length MERS-CoV spike to exclude the possibility that the

493 inhibition by thiosemicarbazide analogs is due to promiscuous binding, which may not exist
494 for the full-length spike. The modified thiosemicarbazides strongly inhibited the pseudovirus
495 infection with EC₅₀ values of 0.91 μM and 0.19 μM for **1g-8** and **1j**, respectively (**Fig. 2b**). This
496 data revalidates our alpha conditions and clearly shows that the tested thiosemicarbazide
497 analogs inhibit the interaction between spike and its receptor hDPP4.

498 Next, we wanted to further test the identified compounds using MERS-CoV. To obtain
499 quantitative values of antiviral activity, we introduced an image-based MERS-CoV infection
500 assay (Ko et al., 2021) in which Vero cells were treated with thiosemicarbazide compounds
501 for 2 hours, followed by MERS-CoV infection at an MOI of 0.0625, after which the viral infection
502 was measured using a fluorescence signal from a immunohistochemical reaction using an
503 anti-spike antibody (**Fig. 3a**). As shown in **Fig. S3**, the immunofluorescence signal is quenched
504 in a concentration-dependent manner in the presence of known antiviral drugs, chloroquine
505 and lopinavir (de Wilde et al., 2014). Our compounds were also found to be highly potent
506 against MERS-CoV infection, and **1j** showed a particularly outstanding EC₅₀ value of 0.73 μM
507 (**Fig. 2b**). To further analyze the antiviral activity of **1g-8** and **1j** in the host cell, we quantified
508 expression of the E protein gene (*upE*) of MERS-CoV using quantitative real-time PCR upon
509 treatment with the compounds (**Fig. S4**). As we expected, the treatment of compounds
510 resulted in a dramatic decrease in the *upE* gene transcript levels compared to that of the
511 untreated cells (**Fig. 3b**), suggesting that the compounds inhibited the entry of MERS-CoV,
512 thereby preventing viral proliferation in the host cell.

513

514 **3.4. Docking analysis of thiosemicarbazides reveals mechanism of action of inhibition**

515 To better understand the mechanism of action, molecular docking of the selected analogs, **1g-**
516 **8** and **1j**, along with **1** was performed on the apo-RBD (PDB: 4L3N) (Chen et al., 2013). As
517 shown in **Fig. 3c**, compound **1** fits well into a pocket of the concave surface of the RBD which
518 was determined as an RBD–hDPP4 binding interface by X-ray crystallography (PDB: 4L72)
519 (Wang et al., 2013). The docking complex of compound **1**:RBD was superimposed onto the

520 co-crystal structure of hDPP4:RBD, and interestingly the ligand binding site matched the
521 region of hDPP4 interaction with RBD (Thr288, Ala291, Leu94, and Ile295) (**Fig. 3c**). This
522 suggests that compound **1** occupies the binding region of hDPP4, interfering with tight protein-
523 protein interaction between RBD and hDPP4, and that its activity could be modulated by
524 varying the substituent on the thioamide NH while keeping the picolinyl hydrazide moiety intact.
525 The para-chloro phenyl group attached to the thioamide NH of **1** interacts with Trp553 by
526 forming a pi-pi contact and synergistic Cl-aromatic pi interaction. Moreover, the picolinyl
527 hydrazide moiety is involved in pi-cation interaction with Lys502 as well as multiple hydrogen
528 bonds with Glu513 and Arg542 (**Fig. 3d**), which are known to contact both Ala291 and Gln344
529 of hDPP4. By contrast, the corresponding 2-methoxy pyridine of **1j** does not fit into this pocket
530 containing Trp553 due to steric hindrance, as this molecule instead binds in the flipped
531 orientation by forming a pi-cation interaction between 2-methoxy pyridine and Lys502 (**Fig.**
532 **3e**). The binding configurations of **1g-8** are nearly identical to those of compound **1**, supporting
533 similar potency between compound **1** and **1g-8** (**Fig. 2b**). Furthermore, to compare the binding
534 affinity of these compounds, we calculated the docking scores for the top 10 docked poses of
535 each compound using Glide docking outputs (**Fig. S5**). The median of the docking scores of
536 compounds **1**, **1g-8**, and **1j** were -1.61, -1.12, and -0.42 kcal/mol, respectively, which were
537 consistent with the order of biological activity (**1** > **1g-8** >> **1j**). We also calculated the
538 electrostatic complementarity (EC) scores of the compound-RBD complexes, and compound
539 **1** (EC score = 0.184) showed a more electrostatically favorable interaction with RBD than **1j**
540 (EC score = 0.073). Noticeably, the methoxy substituent on the pyridine ring of **1j** provides an
541 electrostatic clash, supporting that **1j** is less suitable for binding to the RBD (**Fig. S6**). Based
542 on the binding configurations of the compounds, we concluded that compound **1** has a
543 mechanism of inhibiting RBD binding to hDPP4, and in this process, the picolinyl hydrazide
544 moiety of **1** is crucial for the potency of the thiosemicarbazide compounds.

545

546 **3.5. Amiodarone (class II) has broad-spectrum antiviral activity against coronaviruses**

547 Among 938 **class II** compounds, amiodarone (**Fig. 1d**), which is one of the most commonly
548 used antiarrhythmic drugs (Andreasen et al., 1981; Chatelain and Laruel, 1985), was found to
549 have outstanding antiviral activity in the pseudovirus screen but marginal or no activity in the
550 alpha test (**Fig. S7a**). We have also tested the potency of amiodarone using the MERS-CoV
551 infection assay (**Fig. 4a** and **S7b**) and viral RNA quantification (**Fig. 4b**). As mentioned earlier,
552 the results from pseudovirus screen and alpha test indicate that amiodarone may not target
553 the direct binding of the spike to its receptor protein but instead target the infection stage post-
554 binding. As a proof-of-concept, we performed a time-of-addition experiment (Daelemans et al.,
555 2011; Jeong et al., 2022; Shin et al., 2022). As shown in **Fig. 4c**, when we treated the Huh-7
556 cells with amiodarone at different time points, amiodarone strongly inhibited the viral infection
557 when added at an early time point (1 hour before or at the time of infection), while it showed a
558 marginal antiviral effect when added at later stages of infection (1~6 hours post-infection).
559 Such stage-selective activity was also observed upon treatment with chloroquine, an antiviral
560 drug that achieves its activity *via* increasing lysosomal pH and subsequently prohibiting the
561 release of infected virus from the lysosome, suggesting the possibility of amiodarone acting
562 with a similar mechanism. Lopinavir, which is known to act on the viral protease involved in
563 viral proliferation post-exit from the endosomes, showed efficacy when added at a relatively
564 later stage of infection compared to chloroquine and amiodarone, again suggesting that
565 amiodarone may act early in viral infection. Amiodarone also showed efficacy against other
566 human coronaviruses; an alphacoronavirus HCoV-229E and a betacoronavirus HCoV-OC43
567 (**Fig. 4d** and **S7c**). In total, amiodarone shows potential as a broad-spectrum treatment option
568 for coronaviruses by targeting the early stage of viral infection possibly affecting the endosome
569 (**Fig. 4e**). This is consistent with previous results that amiodarone, as one of the functional
570 inhibitors of acid sphingomyelinase (FIASMA), has demonstrated antiviral efficacy (Miller et
571 al., 2012; Naser et al., 2020) (**Fig. 4e**).

572

573 **3.6. Raloxifene and benzothiophene derivatives (class II) inhibit MERS-CoV infection**

574 Another compound that belongs to **class II** was raloxifene. Raloxifene is a selective estrogen
575 receptor modulator (SERM) that was approved by the FDA in 1997 for the treatment and
576 prevention of postmenopausal osteoporosis and cancer (Hernandez et al., 2003; Lewis and
577 Jordan, 2005). In the pseudovirus assay, raloxifene showed strong potency with an EC₅₀ of
578 0.2 μ M with no significant cytotoxic effects, and was found to be potent against MERS-CoV
579 infection confirmed by the infection assay (**Fig. 5a** and **5b**) and viral RNA quantification (**Fig.**
580 **5c**). Raloxifene was also found to be effective against HCoV-229E and HCoV-OC43, indicating
581 its potential as a broad-spectrum coronavirus treatment option (**Fig. 5d** and **S8**). These results
582 are in line with those of others published while this work was under preparation (Allegretti et
583 al., 2022). In addition, similar to amiodarone, raloxifene appeared to be more potent when
584 added at the earlier stages while it showed only marginal efficacy when treated at later stages
585 of infection (**Fig. 5e**). Previous studies have suggested that raloxifene affects host cell lipid
586 metabolism; and as previously reported cholesterol plays a major role in the fluidity of the
587 plasma membrane (Allegretti et al., 2022; Chang et al., 2022; Hong et al., 2021). In addition,
588 recent studies show that antiviral activity can be achieved by the conversion of cholesterol to
589 25-hydroxycholesterol by CH25H (Schoggins and Randall, 2013; York et al., 2015; Zu et al.,
590 2020). Thus, we reasoned that raloxifene may have broad-spectrum antiviral activity by
591 modulating the host cell membrane through altering cholesterol metabolism. To test this idea,
592 we treated A549 cells with 10 μ M raloxifene and found a marginal elevation of total cellular
593 cholesterol species (**Fig. 5f**). Among the genes in the cholesterol pathway, we found that the
594 *SQLE* coding squalene epoxidase that converts squalene to 2,3-epoxysqualene was
595 significantly enhanced in its expression upon raloxifene treatment (**Fig. 5g**). These results
596 indicate that alteration of cholesterol metabolism upon raloxifene treatment may be the
597 mechanism of its antiviral activity.

598 Since raloxifene contains a benzothiophene analogue, and since the benzothiophene moiety
599 could be essential for the potency of raloxifene, we decided to further examine other hit
600 compounds with benzothiophene. Importantly, we found that compound **2**, like raloxifene, only

601 had marginal potency in the alpha test but a strong efficacy in the MERS-CoV assay. To further
602 characterize **2**, we performed an SAR study with a panel of benzothiophene derivatives (**Fig.**
603 **6a**). As shown in **Fig. 6b**, our SAR studies revealed that the phenyl moiety was an essential
604 region for improving the potency of benzothiophene. When we replaced the phenyl group with
605 tetrahydronaphthalene or benzyl group, their efficacy in the MERS-CoV assay was not
606 detectable, although it remained active in the pseudovirus assay, which suggests that the
607 phenyl group is essential for potency against MERS-CoV replication in the host cells. These
608 results led us to explore derivatives including a modification on the phenyl group, and we found
609 that derivatives with modifications of para-halogen residues (I, F, Br) showed improved
610 potency in both the MERS-CoV infection and pseudovirus assays. In particular, **2a-4** with *p*-
611 bromophenyl group showed an improved efficacy against MERS-CoV infection with an EC₅₀
612 value of 0.95 μM. Interestingly, when we modified the benzothiophene scaffold, the potency
613 of derivative **2b** was comparable to that of **2a-1**, while the substitution of the *p*-bromophenyl
614 group of **2a-4** with an ethoxy group completely abolished its potency (**Fig. 6c-e**). This result
615 suggests that the phenyl group of benzothiophene is crucial for its potency.

616

617 **3.7. Class II compounds show strong potency against SARS-CoV and SARS-CoV-2**

618 Next, we sought to test whether the **class II** compounds have antiviral activity against SARS-
619 CoV or SARS-CoV-2. We utilized an image-based SARS-CoV infection assay to test the
620 efficacy of **class II** compounds against SARS-CoV (Jeon et al., 2020). We first treated the
621 Vero cells with compounds for 2 hours and infected the cells with SARS-CoV at an MOI of
622 0.0625, after which the extent of viral infection was measured by immunofluorescence analysis
623 (**Fig. S9**). As we expected for **class II** compounds, raloxifene, amiodarone, and compounds
624 **2a-1** and **2a-4** showed strong potency against SARS-CoV, indicating its potential utility as a
625 broad-spectrum antiviral agent (**Fig. 7a** and **S10**). **Class II** compounds also strongly inhibited
626 SARS-CoV-2 infection as assessed by viral RNA (**Fig. 7b**). Among the compounds,
627 amiodarone showed an outstanding EC₅₀ value of 3.1 μM, which is better than the EC₅₀ of

628 remdesivir (7.2 μM) (**Fig. S11**), a reference antiviral agent for SARS-CoV-2 infection (Eastman
629 et al., 2020). We also found that raloxifene showed strong potency against SARS-CoV-2
630 infection in a cell-based model, as demonstrated in **Fig. 7c**. To further assess the potency of
631 raloxifene against SARS-CoV-2, we performed an *in vivo* SARS-CoV-2 infection experiment
632 using a hamster model (**Fig. 7d**). We used a sublethal dose of SARS-CoV-2 and measured
633 the mRNA of the virus after a two-day infection period in the presence of 12 or 36 mg/kg
634 raloxifene. As shown in **Fig. 7e-7g**, we found that raloxifene inhibited the replication of SARS-
635 CoV-2 in both lung and nasal turbinate at the higher dose, which was consistent with other
636 previously published results (Allegretti et al., 2022). During the infection, we also monitored
637 the activity and the weight of the infected animals: no significant changes were observed in
638 the weight (**Fig. 7h**) and in the activity level or survival rate (**Fig. S12**). Our *in vivo* results with
639 the hamster model validated the potency of raloxifene, and combined with the potency of
640 benzothiophene analogs, show potential for further development of the identified chemical
641 classes as effective broad-spectrum antiviral drugs.

642

643

644 4. Discussion

645 In this study, we have used a cell-based high-throughput screen platform to screen more than
646 20,000 compounds from the FDA-approved compound and pharmacologically active
647 compound libraries for their potency to inhibit infection by the pseudovirus presenting full-
648 length spike of the MERS-CoV. In combination with the alpha test exploiting the RBD of MERS-
649 CoV spike attached to the oxygen donor bead and receptor hDPP4 attached to the oxygen
650 acceptor bead, the identified hits were classified into a group of compounds capable of
651 inhibiting spike-receptor binding (**class I**), and that of compounds presenting antiviral effects
652 by mechanism other than the binding inhibition (**class II**). Among **class I**, thiosemicarbazide,
653 especially its pyridine moiety, was identified as a potent compound that showed efficacy in
654 both our pseudovirus screen and alpha test, for which the mechanism of action was further
655 confirmed by an ELISA test and the cell-based MERS-CoV infection assay.

656 Among **class II** compounds, amiodarone, a most used antiarrhythmic drug, showed potential
657 as an effective broad-spectrum antiviral against various coronaviruses possibly by targeting
658 the endosomal survival of the virus. As noted, amiodarone, as one of the FIASMA, has been
659 demonstrated to have inhibitory activity against acid sphingomyelinase in the lysosome,
660 thereby leading to a change in cellular lipid metabolism, which results in the modification of
661 the curvature of the cellular membrane crucial for membrane fusion during viral infection
662 (Kornhuber et al., 2010; Miller et al., 2012; Naser et al., 2020; Schloer et al., 2020).

663 Another potent **class II** compound was raloxifene, an FDA-approved selective estrogen
664 receptor modulator. The antiviral efficacy of raloxifene has been also reported by another
665 group while this work was under preparation (Allegretti et al., 2022). Other reports show that
666 the mechanism of antiviral effect of raloxifene is through change in the content of the
667 cytoplasmic membrane or lipid raft, and a recent study shows that the antiviral activity can be
668 achieved by the conversion of cholesterol to 25-hydroxycholesterol by CH25H (Schoggins and
669 Randall, 2013; York et al., 2015; Zu et al., 2020). Although our results do not show alteration
670 in the *CH25H* gene, we demonstrate change in *SQLE* also involved in cholesterol metabolism

671 which confirms the role of modulation of cholesterol metabolism in antiviral efficacy of
672 raloxifene. Also, raloxifene and analogs of benzothiophene, a moiety found in raloxifene,
673 showed efficacy against SARS-CoV and SARS-CoV-2 infection. Especially, treatment with the
674 dose of 36 mg/kg of raloxifene showed a potency against SARS-CoV-2 in a hamster model.
675 Such *in vivo* efficacy of raloxifene was also reported by others in a previously published work
676 (Allegretti et al., 2022).

677 Prophylactic vaccines against SARS-CoV-2 infection are not yet widely available worldwide,
678 thus leading to concern for the unvaccinated population. Coronaviruses can also easily
679 develop genetic mutations necessary to avoid the current vaccines. Antiviral therapeutics can
680 provide a safer and effective way to cure infections caused by both current and future evolving
681 variants. Currently, several neutralizing antibodies and target-specific drugs against SARS-
682 CoV-2, including ritonavir-boosted nirmatrelvir and molnupiravir, have been introduced in the
683 clinical setting, but clinical failure caused by a rebound problem after treatment with those
684 drugs is becoming increasingly common. Our approach shows that drug repositioning and a
685 pseudovirus assay combined with an alpha test can be used to rapidly identify active
686 compounds that can effectively prevent viral infection. Importantly, through our screening
687 platform, we were able to not only identify several compounds as potential broad-spectrum
688 inhibitors against the coronaviruses but also rapidly specify the potential antiviral mechanisms
689 of action. Especially, our results show that amiodarone, raloxifene, and benzothiophene drugs
690 have the potential to be further developed into broad-spectrum antiviral therapeutic options
691 against coronavirus infection.

692

693

694

695

696

697

698 **Declaration of competing interest**

699 The authors declare no competing interests.

700

701 **Appendix A. Supplementary data**

702 The following is the supplementary data to this article.

703

704 **Acknowledgements**

705 The authors thank all members of the Wonsik Lee lab and Bio Center of Gyeonggido Business
706 and Science Accelerator for scientific and experimental discussion.

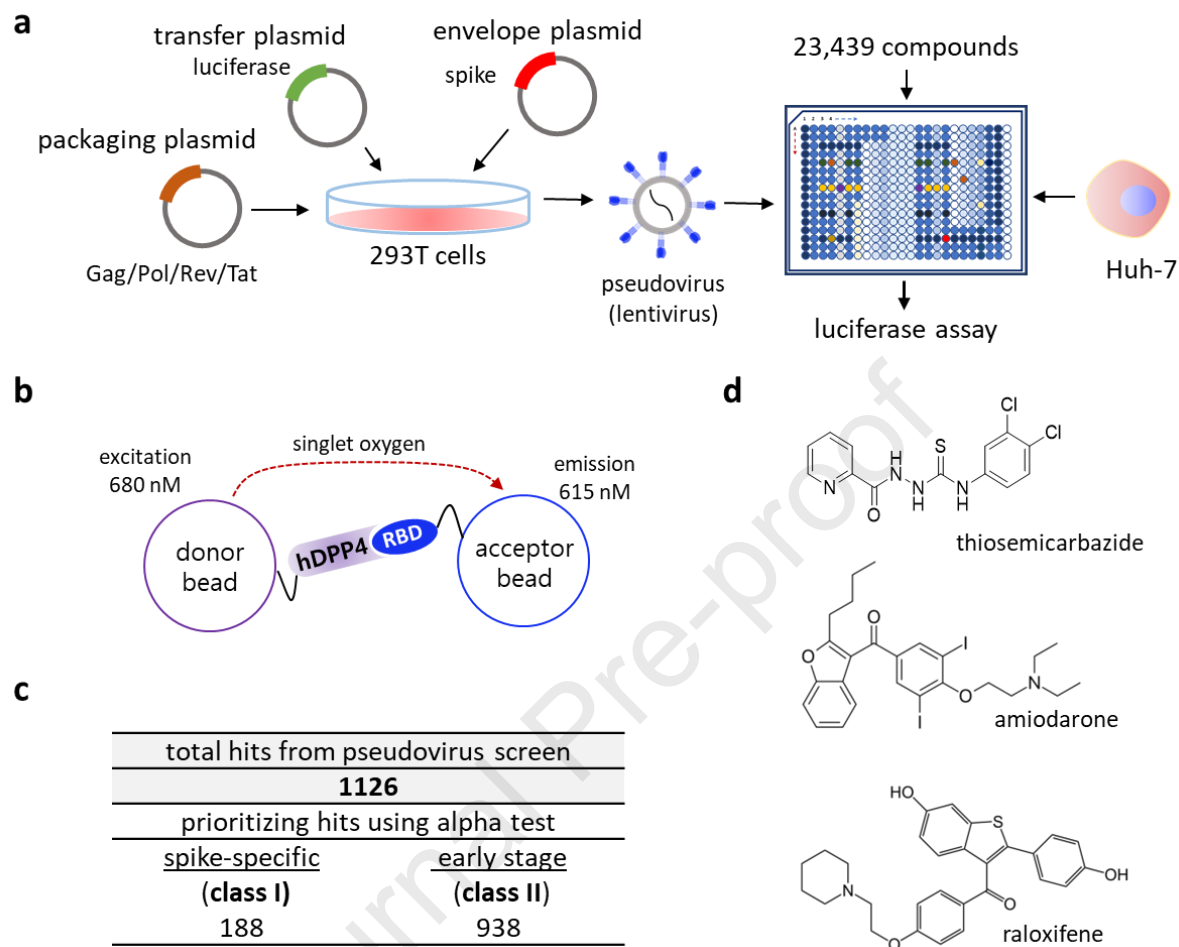
707

708 **Funding Source**

709 This work was supported by a grant from an R&D support program of the Gyeonggi provincial
710 government to KJ; grants from Korea Disease Control and Prevention Agency (KCDC 2021-
711 ER1602-00) and National Research Foundation (NRF) of Korea (NRF-2019R1F1A1060071)
712 to WL; grant funded by NRF of Korea (NRF-2020R1A6A1A03042854) and an Institute of
713 Information & Communications Technology Planning & Evaluation (IITP) grant funded by the
714 Korean government (MSIT) (No. 2020-0-01343) to TN; NRF grants funded by the Korean
715 government (MSIT) (NRF-2017M3A9G6068245 and NRF-2022M3A9J1081343) to SK; NRF
716 grants funded by the Korean government (MSIT) (NRF-2014M3A9D5A01075128,
717 2020M3A9I2109027, 2021M3H9A1030260) to JKS; and a grant funded by Korea Disease
718 Control and Prevention Agency (KCDC-2020-NI-039-00) to JL.

719

720

721 **Figure Legends**

722

723 **Fig. 1. Combination of a pseudovirus assay and protein-based assays enabled**
 724 **identification of novel inhibitors targeting the early stage of coronavirus infection. a)**

725 Schematic representation of a compound screen using a pseudovirus presenting the spike of
 726 MERS-CoV. To generate the pseudovirus, a lentivirus backbone, luciferase gene, and the

727 spike were transfected onto 293T cells. In the compound screen, Huh-7 cells were treated

728 with compounds and infected with the pseudovirus, after which the accumulated luciferase

729 signal was measured. **b)** Schematic representation of the alpha test. In the alpha test, the

730 receptor binding domain (RBD) of the spike of MERS-CoV was immobilized on the donor bead

731 while its cellular receptor, hDPP4 was attached to an acceptor bead. **c)** Summary of

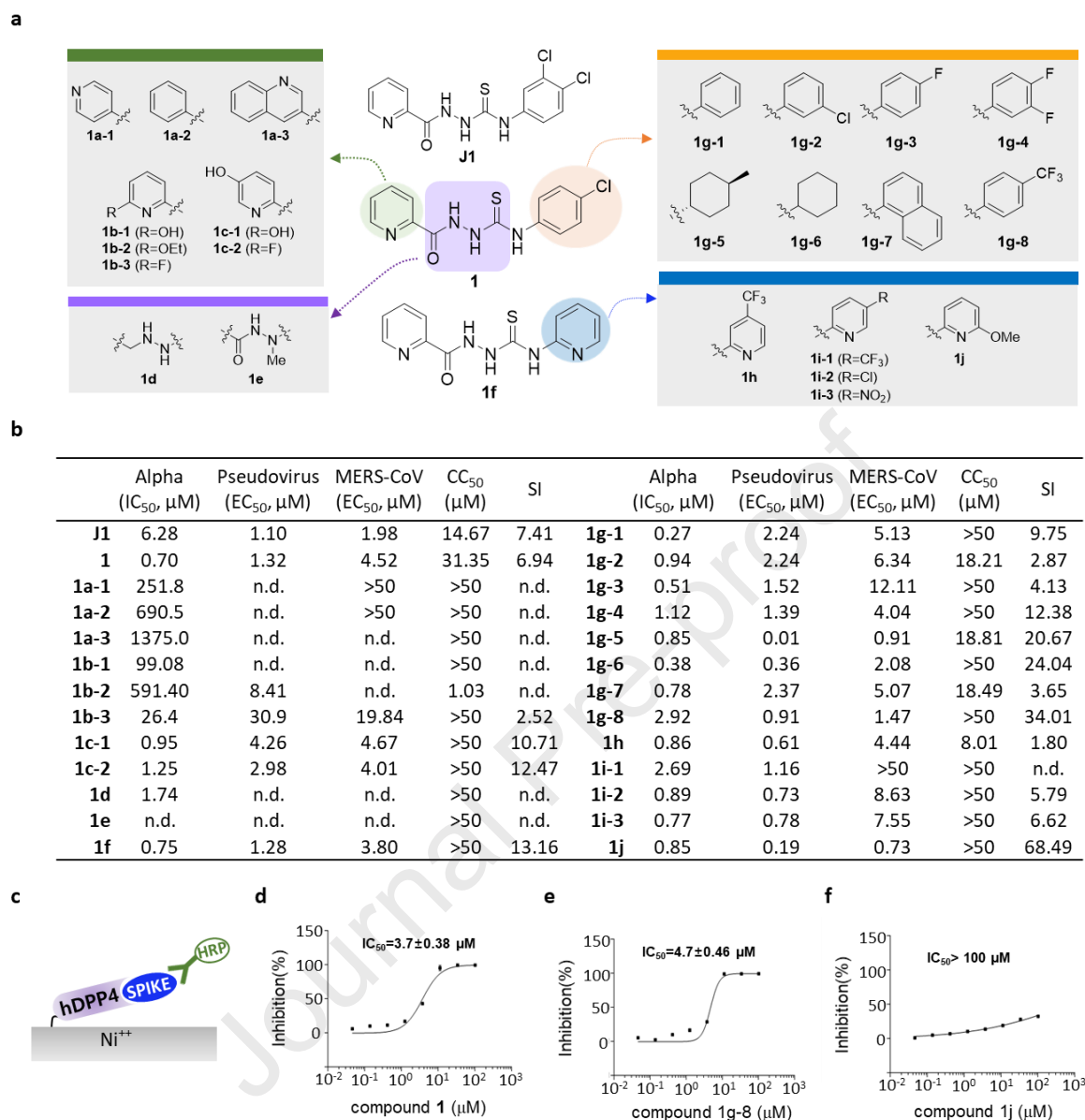
732 classification of hits from the pseudovirus screen and subsequent alpha test: ~16% entry-

733 specific (spike-specific) compounds among 1126 hits. **d)** Structure of three identified hits:

734 thiosemicarbazide, amiodarone, and raloxifene.

735

Journal Pre-proof



736

737 **Fig. 2. Thiosemicarbazide (class I) shows target specificity, and its analogues show**738 **regions for their antiviral potency. a) Structure of newly-synthesized thiosemicarbazide**739 **derivatives. The modified moieties compared to compound 1 or 1f are highlighted in green (2-**740 **pyridine), purple (thiosemicarbazide), orange (pyridine), and blue (*p*-trifluoromethylphenyl).**741 **Potency (IC₅₀ or EC₅₀ (μM)), cytotoxicity (CC₅₀ (μM)), and selective index (SI = CC₅₀ / EC₅₀**742 **(MERS-CoV infection assay)) of thiosemicarbazide derivatives as evaluated in alpha test,**743 **pseudovirus assay, and immunofluorescence-based MERS-CoV infection assay. CC₅₀ values**744 **that are >50 μM were considered as 50 μM when calculating SI. n.d.; not determined. c)**

745 Schematic presentation of the ELISA using hDPP4 and the RBD of the S1 of MERS-CoV spike.
746 **d-f)** Three compounds, **1 (d)**, **1g-8 (e)**, and **1j (f)** tested for their inhibiting activity on the binding
747 between hDPP4 and RBD. Each data point represents the mean of triplicate assays with
748 \pm SEM, and their IC_{50} values were calculated through curve fitting analysis using Prism 6.0.

749

750

751

752

753

754

755

756

757

758

759

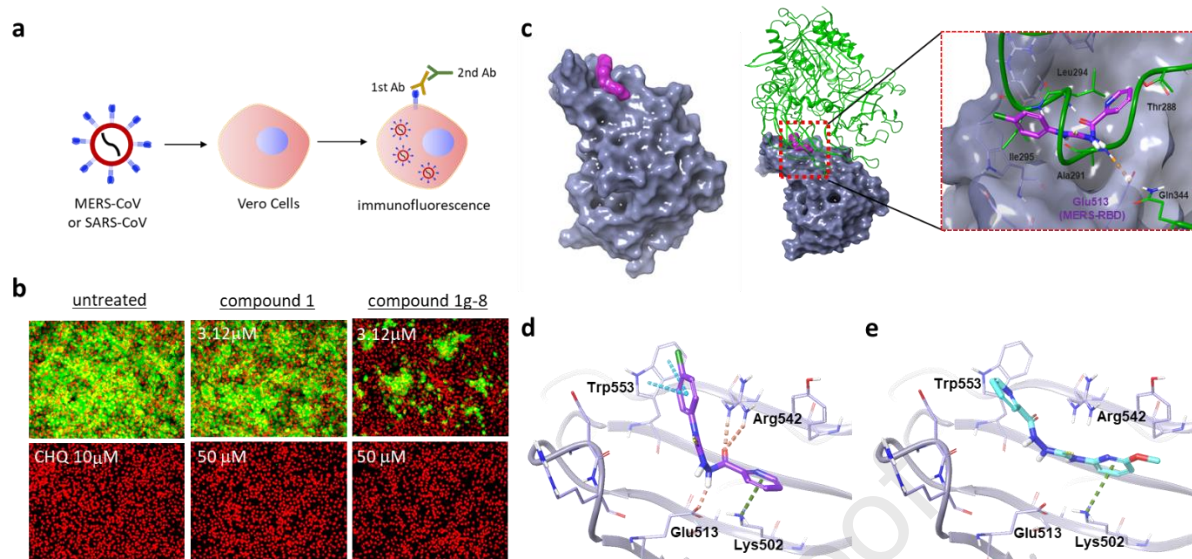
760

761

762

763

764



765

766 **Fig. 3. Thiosemicarbazide inhibits MERS-CoV infection by blocking the interaction**767 **between RBD and hDPP4. a)** Schematic presentation of immunofluorescence-based MERS-768 CoV infection assay. **b)** Antiviral potency of compound **1** and **1g-8** against MERS-CoV

769 infection. The cells were treated with individual compounds at the time of MERS-CoV infection

770 at an MOI of 0.0625. The cells were further incubated for 24 hours followed by

771 immunofluorescence imaging. MERS-CoV infection was determined using a rabbit anti-

772 MERS-CoV spike antibody (green), and cell viability was measured with Hoechst 33342 (red).

773 Concentrations of 3.125 μM and 50 μM were respectively selected as the low and high doses

774 for each compound. Chloroquine (CHQ) at a concentration of 10 μM was included as a control.

775 **c-left)** Docking models for compounds **1** and **1j** bound to the MERS-CoV receptor binding

776 domain (RBD) (PDB: 4L3N). The molecular surface of MERS-CoV RBD is presented in gray

777 while compound **1** is marked in magenta. **c-right)** Superimposition of the RBD docked with **1**

778 (the model in left) on the X-ray structure of RBD complexed with hDPP4 (PDB: 4L72). The

779 gray molecular surface is MERS-CoV RBD (PDB id: 4L3N, 4L72) and the green ribbon is

780 hDPP4. **d-e)** Comparison of docked configurations of **1** (**d**) and **1j** (**e**) to the binding site in the

781 RBD. Key interactions between ligand and RBD are presented by dashed lines: orange is a

782 hydrogen bond, cyan is a pi-pi interaction, and green is a pi-cation interaction. Ligands are

783 colored by atom types, with carbon as magenta in **1**, cyan in **1j**, and silver in RBD; nitrogen is

784 blue; oxygen is red; and fluorine is green.

785

786

787

788

789

790

791

792

793

794

795

796

797

798

799

800

801

802

803

804

805

806

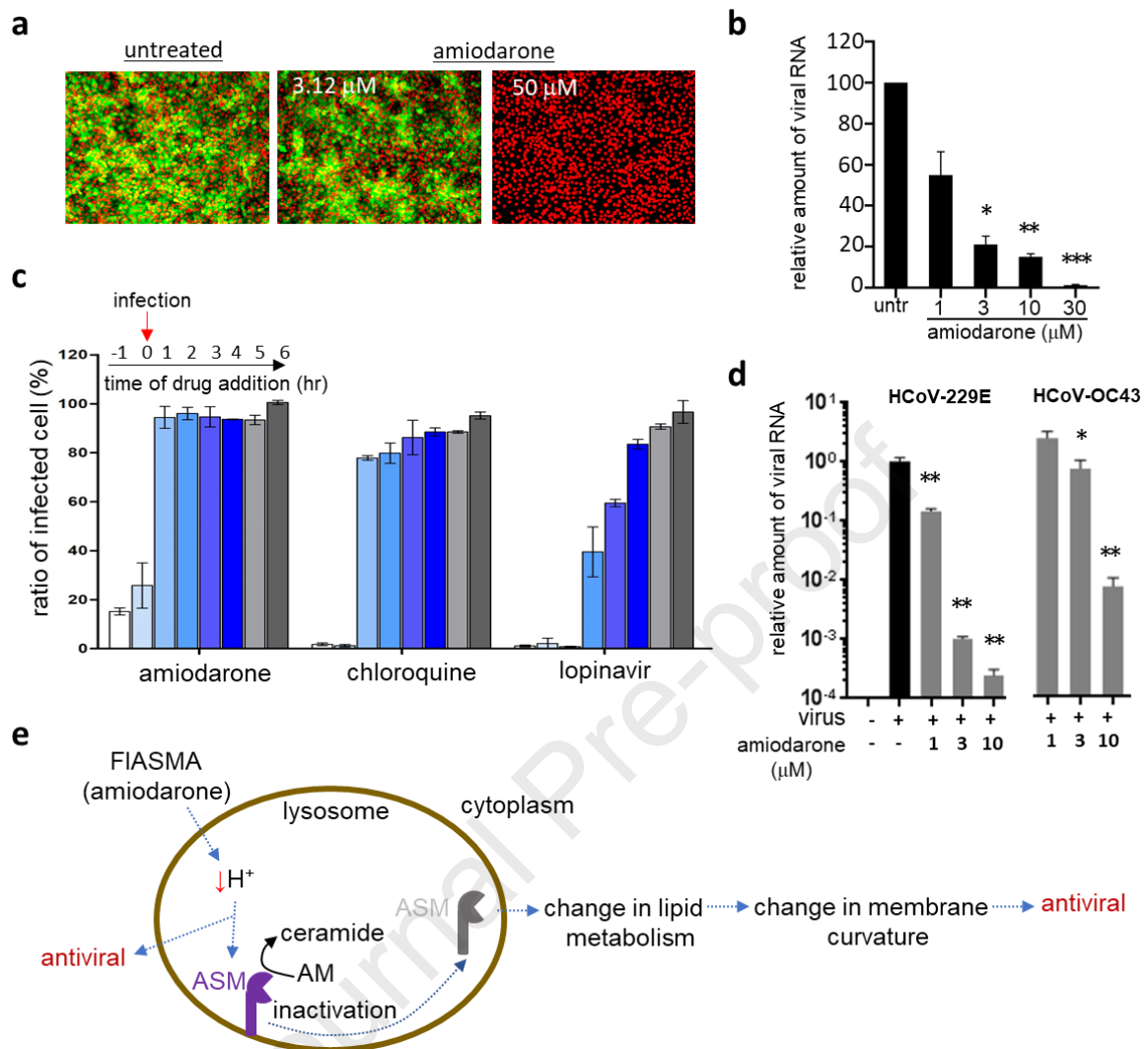
807

808

809

810

Journal Pre-proof



811

812 **Fig. 4. Amiodarone (class II) inhibits the early stage of coronavirus infection.**

813 antiviral activity of amiodarone demonstrated by an immunofluorescence-based MERS-CoV infection

814 assay. In total, ten different concentrations (1~50 μ M) of amiodarone were examined, and815 immunofluorescence images obtained from low (3.12 μ M) and high (50 μ M) compound

816 concentrations were selected. Green signals represent cells infected with MERS-CoV and red

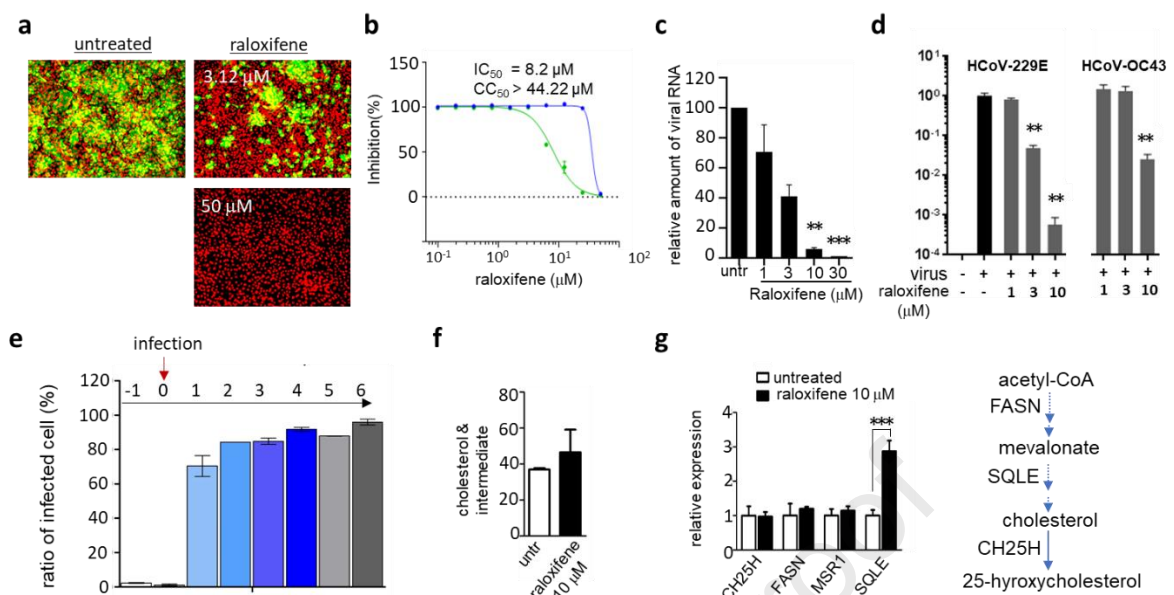
817 signals indicate cell survival. **b**) Viral mRNA from cells infected with MERS-CoV quantified by818 qRT-PCR. Each data point represents the mean \pm SEM of triplicate assays. **c**) Time-of-addition819 experiment performed by addition of 10 μ M amiodarone at different time points during MERS-

820 CoV infection. Drugs were added at one hour before infection (-1), at the time of infection (0),

821 or at various hours post-infection (+1 ~ +6), and the extent of inhibition of the MERS-CoV

822 infection was quantified by the immunofluorescence signals. Chloroquine and lopinavir were
823 included at a concentration of 10 μ M for comparison. Each data point represents the mean \pm
824 SEM of triplicate assays. **d)** Antiviral activity of amiodarone examined against the HCoV-229E
825 and HCoV-OC43 viruses. Viruses were infected into Vero cells in the presence of amiodarone,
826 and after 24 hours of infection, viral mRNA was quantified by qRT-PCR. Each data point
827 represents the mean \pm SEM of triplicate assays. **e)** Graphical presentation of potential
828 mechanisms of the antiviral activity of amiodarone. Amiodarone, as a weak base, could lead
829 to an alkalization of the lysosome and therefore act as a potential inhibitor of lysosomal acid
830 sphingomyelinase. ASM, acid-sphingomyelinase; AM, acid-sphingomyelin.

831



832

833 **Fig. 5. Raloxifene inhibits the early stage of coronavirus infection. a)** Antiviral activity of

834 raloxifene demonstrated by an immunofluorescence-based MERS-CoV infection assay as

835 previously noted in **Fig. 4a**. Green signals represent cells infected with MERS-CoV and red836 signals represent cell survival. **b)** In total, ten different concentrations of raloxifene were tested837 in the immunofluorescence assay, and EC_{50} and cytotoxicity were calculated through curve838 fitting analysis using Prism 6. **c)** Viral mRNA quantified by qRT-PCR from the Vero cells839 infected with MERS-CoV. **d)** Potency of raloxifene against HCoV-229E or HCoV-OC43840 measured by qRT-PCR as detailed in **Fig. 4d**. **e)** Time-of-addition experiment using 10 μM of841 raloxifene. Experiments were performed as described in **Fig. 4c**. **f)** Cellular cholesterol levels842 in A549 cells treated with 10 μM raloxifene for 12 hours. **g)** Expression levels of selected

843 genes involved in cholesterol metabolism quantified by qRT-PCR after 12 hours of treatment

844 with 10 μM raloxifene. CH25H; cholesterol 25-Hydroxylase, FASN; fatty acid synthase, MSR1;

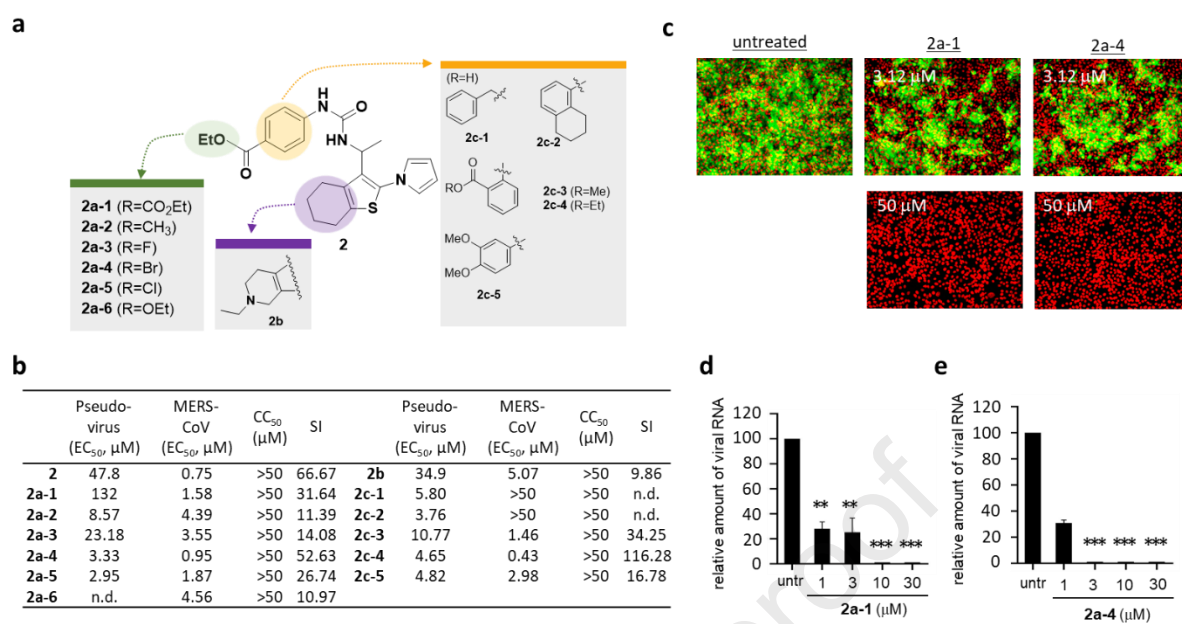
845 macrophage scavenger receptor 1, SQLE; squalene epoxidase. Each data point represents

846 the mean \pm SEM of triplicate assays.

847

848

849



850

851 **Fig. 6. Benzothiophene analogues (class II) show regions crucial for antiviral potency.**852 **a)** Structure activity relationship (SAR) analysis performed using newly synthesized853 benzothiophene derivatives. The modified moieties of the phenyl group of compound **2** are854 highlighted in green or orange color, and the thiophene moiety is highlighted in purple. **b)**855 Potency (EC₅₀ (μM)) of tested benzothiophene derivatives evaluated by MERS-CoV

856 pseudovirus assay and immunofluorescence-based MERS-CoV infection assay, cytotoxicity

857 (CC₅₀ (μM)), and selective index (SI = CC₅₀ / EC₅₀ (MERS-CoV infection assay)). CC₅₀ values858 that are >50 μM were considered as 50 μM when calculating SI. n.d.; not determined. **c)**859 Antiviral activity of **2a-1** and **2a-4** examined by immunofluorescence-based MERS-CoV860 infection assay as noted in **Fig. 4a**. Green signals present the cells infected with MERS-CoV861 and red signals present all cells. **d-e)** Antiviral potency of **2a-1** (**d**) and **2a-4** (**e**) against HCoV-862 229E or HCoV-OC43 measured by qRT-PCR as noted in **Fig. 4d**. Each data point represents

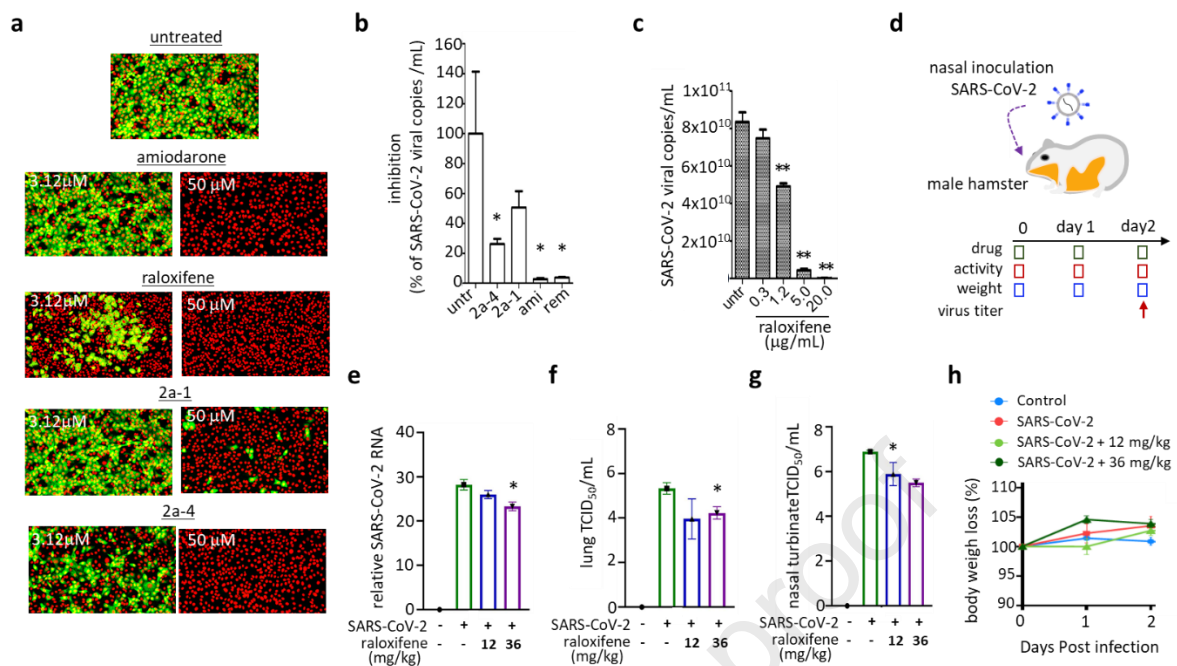
863 the mean of triplicate assays with ±SEM.

864

865

866

867



868

869 **Fig. 7. Compounds inhibiting the early stage of coronavirus infection show potency**870 **against both SARS-CoV and SARS-CoV-2 infection. a)** Antiviral activity of the selected871 **broad-spectrum compounds (amiodarone, raloxifene, 2a-1, and 2a-4) demonstrated by**872 **immunofluorescence-based SARS-CoV infection assay. Among the ten different**873 **concentrations (1~50 μM) of each compound examined, images at low (3.12 μM) and high (50**874 **μM) concentrations were selected. Green signals represent cells infected with SARS-CoV and**875 **red signals represent cell survival. b-c)** Potency of the selected drugs against SARS-CoV2876 **infection demonstrated with a cell-based infection model. Cells were treated with 10 μM of**877 **amiodarone, 2a-1, and 2a-4 (b), raloxifene (c) at the time of infection with SARS-CoV-2, and**878 **viral mRNA was quantified by qRT-PCR after 24 hours of infection. For comparison, 10 μM of**879 **remdesivir was included. d-g) *In vivo* potency of raloxifene against SARS-CoV-2**880 **demonstrated using a hamster infection model. d)** Schematic presentation of SARS-CoV2881 **infection and sampling. SARS-CoV-2 was infected through nasal inoculation and animals were**882 **treated with raloxifene during a two-day infection period at 12 mg/kg or 36 mg/kg doses. On**883 **day 2, viral titer in the hamsters was measured by qRT-PCR. e-f)** Viral titers of SARS-CoV-2884 **in lungs quantified on day 2 by qRT-PCR (e) or TCID₅₀ (f). g)** Viral titer of nasal turbinate

885 quantified on day 2 by TCID₅₀. **h)** Body weight of the hamsters was measured daily for the 2-
886 day infection period and they remained normal. Each data point represents the mean \pm SEM
887 of triplicate assays.

888

889

890

891

892

893

894

895

896

897

898

899

900

901

902

903

904

905

906

907

908

909

910

911

912 **References**

- 913 Allegretti, M., Cesta, M.C., Zippoli, M., Beccari, A., Talarico, C., Mantelli, F., Bucci, E.M., Scorzolini, L.,
914 Nicastri, E., 2022. Repurposing the estrogen receptor modulator raloxifene to treat SARS-CoV-2
915 infection. *Cell Death Differ* 29, 156-166.
- 916 Andersen, K.G., Rambaut, A., Lipkin, W.I., Holmes, E.C., Garry, R.F., 2020. The proximal origin of SARS-
917 CoV-2. *Nat Med* 26, 450-452.
- 918 Andreasen, F., Agerbaek, H., Bjerregaard, P., Gotzsche, H., 1981. Pharmacokinetics of amiodarone
919 after intravenous and oral administration. *Eur J Clin Pharmacol* 19, 293-299.
- 920 Bosch, B.J., Martina, B.E., Van Der Zee, R., Lepault, J., Haijema, B.J., Versluis, C., Heck, A.J., De Groot,
921 R., Osterhaus, A.D., Rottier, P.J., 2004. Severe acute respiratory syndrome coronavirus (SARS-CoV)
922 infection inhibition using spike protein heptad repeat-derived peptides. *Proc Natl Acad Sci U S A*
923 101, 8455-8460.
- 924 Burkard, C., Verheije, M.H., Wicht, O., van Kasteren, S.I., van Kuppeveld, F.J., Haagmans, B.L., Pelkmans,
925 L., Rottier, P.J., Bosch, B.J., de Haan, C.A., 2014. Coronavirus cell entry occurs through the endo-
926 /lysosomal pathway in a proteolysis-dependent manner. *PLoS Pathog* 10, e1004502.
- 927 Campeau, E., Ruhl, V.E., Rodier, F., Smith, C.L., Rahmberg, B.L., Fuss, J.O., Campisi, J., Yaswen, P., Cooper,
928 P.K., Kaufman, P.D., 2009. A versatile viral system for expression and depletion of proteins in
929 mammalian cells. *PLoS One* 4, e6529.
- 930 Chang, J., Kim, J., Lee, W., 2022. Raloxifene prevents intracellular invasion of pathogenic bacteria
931 through modulation of cell metabolic pathways. *J Antimicrob Chemother* 77, 1617-1624.
- 932 Chatelain, P., Laruel, R., 1985. Amiodarone partitioning with phospholipid bilayers and erythrocyte
933 membranes. *J Pharm Sci* 74, 783-784.
- 934 Che, L., Chi, W., Qiao, Y., Zhang, J., Song, X., Liu, Y., Li, L., Jia, J., Pilo, M.G., Wang, J., Cigliano, A., Ma,
935 Z., Kuang, W., Tang, Z., Zhang, Z., Shui, G., Ribback, S., Dombrowski, F., Evert, M., Pascale, R.M., Cossu,
936 C., Pes, G.M., Osborne, T.F., Calvisi, D.F., Chen, X., Chen, L., 2020. Cholesterol biosynthesis supports
937 the growth of hepatocarcinoma lesions depleted of fatty acid synthase in mice and humans. *Gut* 69,
938 177-186.
- 939 Cheeseright, T., Mackey, M., Rose, S., Vinter, A., 2006. Molecular field extrema as descriptors of
940 biological activity: definition and validation. *J Chem Inf Model* 46, 665-676.
- 941 Chen, Y., Rajashankar, K.R., Yang, Y., Agnihothram, S.S., Liu, C., Lin, Y.L., Baric, R.S., Li, F., 2013. Crystal
942 structure of the receptor-binding domain from newly emerged Middle East respiratory syndrome
943 coronavirus. *J Virol* 87, 10777-10783.
- 944 Corman, V.M., Eckerle, I., Bleicker, T., Zaki, A., Landt, O., Eschbach-Bludau, M., van Boheemen, S.,
945 Gopal, R., Ballhause, M., Bestebroer, T.M., Muth, D., Muller, M.A., Drexler, J.F., Zambon, M., Osterhaus,
946 A.D., Fouchier, R.M., Drosten, C., 2012. Detection of a novel human coronavirus by real-time reverse-
947 transcription polymerase chain reaction. *Euro Surveill* 17.
- 948 Cui, J., Li, F., Shi, Z.L., 2019. Origin and evolution of pathogenic coronaviruses. *Nat Rev Microbiol* 17,
949 181-192.

- 950 Daelemans, D., Pauwels, R., De Clercq, E., Pannecouque, C., 2011. A time-of-drug addition approach
951 to target identification of antiviral compounds. *Nat Protoc* 6, 925-933.
- 952 de Wilde, A.H., Jochmans, D., Posthuma, C.C., Zevenhoven-Dobbe, J.C., van Nieuwkoop, S., Bestebroer,
953 T.M., van den Hoogen, B.G., Neyts, J., Snijder, E.J., 2014. Screening of an FDA-approved compound
954 library identifies four small-molecule inhibitors of Middle East respiratory syndrome coronavirus
955 replication in cell culture. *Antimicrob Agents Chemother* 58, 4875-4884.
- 956 Eastman, R.T., Roth, J.S., Brimacombe, K.R., Simeonov, A., Shen, M., Patnaik, S., Hall, M.D., 2020.
957 Remdesivir: A Review of Its Discovery and Development Leading to Emergency Use Authorization
958 for Treatment of COVID-19. *ACS Cent Sci* 6, 672-683.
- 959 Eurosurveillance Editorial, T., 2020. Note from the editors: World Health Organization declares novel
960 coronavirus (2019-nCoV) sixth public health emergency of international concern. *Euro Surveill* 25.
- 961 Fuentes-Prior, P., 2021. Priming of SARS-CoV-2 S protein by several membrane-bound serine
962 proteinases could explain enhanced viral infectivity and systemic COVID-19 infection. *J Biol Chem*
963 296, 100135.
- 964 Geller, C., Varbanov, M., Duval, R.E., 2012. Human coronaviruses: insights into environmental
965 resistance and its influence on the development of new antiseptic strategies. *Viruses* 4, 3044-3068.
- 966 Guan, Y., Zheng, B.J., He, Y.Q., Liu, X.L., Zhuang, Z.X., Cheung, C.L., Luo, S.W., Li, P.H., Zhang, L.J., Guan,
967 Y.J., Butt, K.M., Wong, K.L., Chan, K.W., Lim, W., Shortridge, K.F., Yuen, K.Y., Peiris, J.S., Poon, L.L., 2003.
968 Isolation and characterization of viruses related to the SARS coronavirus from animals in southern
969 China. *Science* 302, 276-278.
- 970 Hartenian, E., Nandakumar, D., Lari, A., Ly, M., Tucker, J.M., Glaunsinger, B.A., 2020. The molecular
971 virology of coronaviruses. *J Biol Chem* 295, 12910-12934.
- 972 Hernandez, E., Valera, R., Alonzo, E., Bajares-Lilue, M., Carlini, R., Capriles, F., Martinis, R., Bellorin-
973 Font, E., Weisinger, J.R., 2003. Effects of raloxifene on bone metabolism and serum lipids in
974 postmenopausal women on chronic hemodialysis. *Kidney Int* 63, 2269-2274.
- 975 Hong, S., Chang, J., Jeong, K., Lee, W., 2021. Raloxifene as a treatment option for viral infections. *J*
976 *Microbiol* 59, 124-131.
- 977 Hu, B., Guo, H., Zhou, P., Shi, Z.L., 2021. Characteristics of SARS-CoV-2 and COVID-19. *Nat Rev*
978 *Microbiol* 19, 141-154.
- 979 Huang, C., Wang, Y., Li, X., Ren, L., Zhao, J., Hu, Y., Zhang, L., Fan, G., Xu, J., Gu, X., Cheng, Z., Yu, T.,
980 Xia, J., Wei, Y., Wu, W., Xie, X., Yin, W., Li, H., Liu, M., Xiao, Y., Gao, H., Guo, L., Xie, J., Wang, G., Jiang,
981 R., Gao, Z., Jin, Q., Wang, J., Cao, B., 2020. Clinical features of patients infected with 2019 novel
982 coronavirus in Wuhan, China. *Lancet* 395, 497-506.
- 983 Jeon, S., Ko, M., Lee, J., Choi, I., Byun, S.Y., Park, S., Shum, D., Kim, S., 2020. Identification of Antiviral
984 Drug Candidates against SARS-CoV-2 from FDA-Approved Drugs. *Antimicrob Agents Chemother* 64.
- 985 Jeong, K., Kim, J., Chang, J., Hong, S., Kim, I., Oh, S., Jeon, S., Lee, J.C., Park, H.J., Kim, S., Lee, W., 2022.
986 Chemical screen uncovers novel structural classes of inhibitors of the papain-like protease of
987 coronaviruses. *iScience* 25, 105254.
- 988 Klopffleisch, R., 2013. Multiparametric and semiquantitative scoring systems for the evaluation of

- 989 mouse model histopathology--a systematic review. *BMC Vet Res* 9, 123.
- 990 Ko, M., Chang, S.Y., Byun, S.Y., Ianevski, A., Choi, I., Pham Hung d'Alexandry d'Orengiani, A.L., Ravlo,
991 E., Wang, W., BJORAS, M., Kainov, D.E., Shum, D., Min, J.Y., Windisch, M.P., 2021. Screening of FDA-
992 Approved Drugs Using a MERS-CoV Clinical Isolate from South Korea Identifies Potential Therapeutic
993 Options for COVID-19. *Viruses* 13.
- 994 Kornhuber, J., Tripal, P., Reichel, M., Muhle, C., Rhein, C., Muehlbacher, M., Groemer, T.W., Gulbins, E.,
995 2010. Functional Inhibitors of Acid Sphingomyelinase (FIASMAS): a novel pharmacological group of
996 drugs with broad clinical applications. *Cell Physiol Biochem* 26, 9-20.
- 997 Krammer, F., 2020. SARS-CoV-2 vaccines in development. *Nature* 586, 516-527.
- 998 Ksiazek, T.G., Erdman, D., Goldsmith, C.S., Zaki, S.R., Peret, T., Emery, S., Tong, S., Urbani, C., Comer,
999 J.A., Lim, W., Rollin, P.E., Dowell, S.F., Ling, A.E., Humphrey, C.D., Shieh, W.J., Guarner, J., Paddock, C.D.,
1000 Rota, P., Fields, B., DeRisi, J., Yang, J.Y., Cox, N., Hughes, J.M., LeDuc, J.W., Bellini, W.J., Anderson, L.J.,
1001 Group, S.W., 2003. A novel coronavirus associated with severe acute respiratory syndrome. *N Engl J*
1002 *Med* 348, 1953-1966.
- 1003 Lam, T.T., Jia, N., Zhang, Y.W., Shum, M.H., Jiang, J.F., Zhu, H.C., Tong, Y.G., Shi, Y.X., Ni, X.B., Liao, Y.S.,
1004 Li, W.J., Jiang, B.G., Wei, W., Yuan, T.T., Zheng, K., Cui, X.M., Li, J., Pei, G.Q., Qiang, X., Cheung, W.Y., Li,
1005 L.F., Sun, F.F., Qin, S., Huang, J.C., Leung, G.M., Holmes, E.C., Hu, Y.L., Guan, Y., Cao, W.C., 2020.
1006 Identifying SARS-CoV-2-related coronaviruses in Malayan pangolins. *Nature* 583, 282-285.
- 1007 Lewis, J.S., Jordan, V.C., 2005. Selective estrogen receptor modulators (SERMs): mechanisms of
1008 anticarcinogenesis and drug resistance. *Mutat Res* 591, 247-263.
- 1009 Li, F., 2016. Structure, Function, and Evolution of Coronavirus Spike Proteins. *Annu Rev Virol* 3, 237-
1010 261.
- 1011 Li, F., Li, W., Farzan, M., Harrison, S.C., 2005. Structure of SARS coronavirus spike receptor-binding
1012 domain complexed with receptor. *Science* 309, 1864-1868.
- 1013 Li, Q., Guan, X., Wu, P., Wang, X., Zhou, L., Tong, Y., Ren, R., Leung, K.S.M., Lau, E.H.Y., Wong, J.Y., Xing,
1014 X., Xiang, N., Wu, Y., Li, C., Chen, Q., Li, D., Liu, T., Zhao, J., Liu, M., Tu, W., Chen, C., Jin, L., Yang, R.,
1015 Wang, Q., Zhou, S., Wang, R., Liu, H., Luo, Y., Liu, Y., Shao, G., Li, H., Tao, Z., Yang, Y., Deng, Z., Liu, B.,
1016 Ma, Z., Zhang, Y., Shi, G., Lam, T.T.Y., Wu, J.T., Gao, G.F., Cowling, B.J., Yang, B., Leung, G.M., Feng, Z.,
1017 2020. Early Transmission Dynamics in Wuhan, China, of Novel Coronavirus-Infected Pneumonia. *N*
1018 *Engl J Med* 382, 1199-1207.
- 1019 Li, W., Moore, M.J., Vasilieva, N., Sui, J., Wong, S.K., Berne, M.A., Somasundaran, M., Sullivan, J.L.,
1020 Luzuriaga, K., Greenough, T.C., Choe, H., Farzan, M., 2003. Angiotensin-converting enzyme 2 is a
1021 functional receptor for the SARS coronavirus. *Nature* 426, 450-454.
- 1022 Liu, I.J., Kao, C.L., Hsieh, S.C., Wey, M.T., Kan, L.S., Wang, W.K., 2009. Identification of a minimal
1023 peptide derived from heptad repeat (HR) 2 of spike protein of SARS-CoV and combination of HR1-
1024 derived peptides as fusion inhibitors. *Antiviral Res* 81, 82-87.
- 1025 Miller, M.E., Adhikary, S., Kolokoltssov, A.A., Davey, R.A., 2012. Ebolavirus requires acid
1026 sphingomyelinase activity and plasma membrane sphingomyelin for infection. *J Virol* 86, 7473-7483.
- 1027 Naser, E., Kadow, S., Schumacher, F., Mohamed, Z.H., Kappe, C., Hessler, G., Pollmeier, B., Kleuser, B.,

- 1028 Arenz, C., Becker, K.A., Gulbins, E., Carpinteiro, A., 2020. Characterization of the small molecule ARC39,
1029 a direct and specific inhibitor of acid sphingomyelinase in vitro. *J Lipid Res* 61, 896-910.
- 1030 Niu, P., Shen, J., Zhu, N., Lu, R., Tan, W., 2016. Two-tube multiplex real-time reverse transcription PCR
1031 to detect six human coronaviruses. *Virology* 51, 85-88.
- 1032 Park, Y.J., Walls, A.C., Wang, Z., Sauer, M.M., Li, W., Tortorici, M.A., Bosch, B.J., DiMaio, F., Veesler, D.,
1033 2019. Structures of MERS-CoV spike glycoprotein in complex with sialoside attachment receptors.
1034 *Nat Struct Mol Biol* 26, 1151-1157.
- 1035 Paules, C.I., Marston, H.D., Fauci, A.S., 2020. Coronavirus Infections-More Than Just the Common
1036 Cold. *JAMA* 323, 707-708.
- 1037 Raj, V.S., Mou, H., Smits, S.L., Dekkers, D.H., Muller, M.A., Dijkman, R., Muth, D., Demmers, J.A., Zaki,
1038 A., Fouchier, R.A., Thiel, V., Drosten, C., Rottier, P.J., Osterhaus, A.D., Bosch, B.J., Haagmans, B.L., 2013.
1039 Dipeptidyl peptidase 4 is a functional receptor for the emerging human coronavirus-EMC. *Nature*
1040 495, 251-254.
- 1041 Raj, V.S., Smits, S.L., Provacia, L.B., van den Brand, J.M., Wiersma, L., Ouwendijk, W.J., Bestebroer, T.M.,
1042 Spronken, M.I., van Amerongen, G., Rottier, P.J., Fouchier, R.A., Bosch, B.J., Osterhaus, A.D., Haagmans,
1043 B.L., 2014. Adenosine deaminase acts as a natural antagonist for dipeptidyl peptidase 4-mediated
1044 entry of the Middle East respiratory syndrome coronavirus. *J Virol* 88, 1834-1838.
- 1045 Rota, P.A., Oberste, M.S., Monroe, S.S., Nix, W.A., Campagnoli, R., Icenogle, J.P., Penaranda, S.,
1046 Bankamp, B., Maher, K., Chen, M.H., Tong, S., Tamin, A., Lowe, L., Frace, M., DeRisi, J.L., Chen, Q.,
1047 Wang, D., Erdman, D.D., Peret, T.C., Burns, C., Ksiazek, T.G., Rollin, P.E., Sanchez, A., Liffick, S., Holloway,
1048 B., Limor, J., McCaustland, K., Olsen-Rasmussen, M., Fouchier, R., Gunther, S., Osterhaus, A.D., Drosten,
1049 C., Pallansch, M.A., Anderson, L.J., Bellini, W.J., 2003. Characterization of a novel coronavirus
1050 associated with severe acute respiratory syndrome. *Science* 300, 1394-1399.
- 1051 Schloer, S., Brunotte, L., Goretzko, J., Mecate-Zambrano, A., Korthals, N., Gerke, V., Ludwig, S., Rescher,
1052 U., 2020. Targeting the endolysosomal host-SARS-CoV-2 interface by clinically licensed functional
1053 inhibitors of acid sphingomyelinase (FIASMA) including the antidepressant fluoxetine. *Emerg*
1054 *Microbes Infect* 9, 2245-2255.
- 1055 Schoggins, J.W., Randall, G., 2013. Lipids in innate antiviral defense. *Cell Host Microbe* 14, 379-385.
- 1056 Schorpp, K., Rothnagler, I., Salmina, E., Reinshagen, J., Low, T., Brenke, J.K., Gopalakrishnan, J., Tetko,
1057 I.V., Gul, S., Hadian, K., 2014. Identification of Small-Molecule Frequent Hitters from AlphaScreen
1058 High-Throughput Screens. *J Biomol Screen* 19, 715-726.
- 1059 Shang, J., Wan, Y., Luo, C., Ye, G., Geng, Q., Auerbach, A., Li, F., 2020. Cell entry mechanisms of SARS-
1060 CoV-2. *Proc Natl Acad Sci U S A* 117, 11727-11734.
- 1061 Shin, Y.H., Jeong, K., Lee, J., Lee, H.J., Yim, J., Kim, J., Kim, S., Park, S.B., 2022. Inhibition of ACE2-Spike
1062 Interaction by an ACE2 Binder Suppresses SARS-CoV-2 Entry. *Angew Chem Int Ed Engl* 61,
1063 e202115695.
- 1064 Song, Z., Xu, Y., Bao, L., Zhang, L., Yu, P., Qu, Y., Zhu, H., Zhao, W., Han, Y., Qin, C., 2019. From SARS
1065 to MERS, Thrusting Coronaviruses into the Spotlight. *Viruses* 11.
- 1066 Stewart, S.A., Dykxhoorn, D.M., Palliser, D., Mizuno, H., Yu, E.Y., An, D.S., Sabatini, D.M., Chen, I.S.,

- 1067 Hahn, W.C., Sharp, P.A., Weinberg, R.A., Novina, C.D., 2003. Lentivirus-delivered stable gene silencing
1068 by RNAi in primary cells. *RNA* 9, 493-501.
- 1069 Tregoning, J.S., Flight, K.E., Higham, S.L., Wang, Z., Pierce, B.F., 2021. Progress of the COVID-19 vaccine
1070 effort: viruses, vaccines and variants versus efficacy, effectiveness and escape. *Nat Rev Immunol* 21,
1071 626-636.
- 1072 Ullman, E.F., Kirakossian, H., Singh, S., Wu, Z.P., Irvin, B.R., Pease, J.S., Switchenko, A.C., Irvine, J.D.,
1073 Dafforn, A., Skold, C.N., et al., 1994. Luminescent oxygen channeling immunoassay: measurement of
1074 particle binding kinetics by chemiluminescence. *Proc Natl Acad Sci U S A* 91, 5426-5430.
- 1075 Wang, H., Yang, P., Liu, K., Guo, F., Zhang, Y., Zhang, G., Jiang, C., 2008. SARS coronavirus entry into
1076 host cells through a novel clathrin- and caveolae-independent endocytic pathway. *Cell Res* 18, 290-
1077 301.
- 1078 Wang, N., Shi, X., Jiang, L., Zhang, S., Wang, D., Tong, P., Guo, D., Fu, L., Cui, Y., Liu, X., Arledge, K.C.,
1079 Chen, Y.H., Zhang, L., Wang, X., 2013. Structure of MERS-CoV spike receptor-binding domain
1080 complexed with human receptor DPP4. *Cell Res* 23, 986-993.
- 1081 Xia, S., Liu, Q., Wang, Q., Sun, Z., Su, S., Du, L., Ying, T., Lu, L., Jiang, S., 2014. Middle East respiratory
1082 syndrome coronavirus (MERS-CoV) entry inhibitors targeting spike protein. *Virus Res* 194, 200-210.
- 1083 Yang, L., Geng, T., Yang, G., Ma, J., Wang, L., Ketkar, H., Yang, D., Lin, T., Hwang, J., Zhu, S., Wang, Y.,
1084 Dai, J., You, F., Cheng, G., Vella, A.T., Flavell, R.A., Fikrig, E., Wang, P., 2020. Macrophage scavenger
1085 receptor 1 controls Chikungunya virus infection through autophagy in mice. *Commun Biol* 3, 556.
- 1086 York, A.G., Williams, K.J., Argus, J.P., Zhou, Q.D., Brar, G., Vergnes, L., Gray, E.E., Zhen, A., Wu, N.C.,
1087 Yamada, D.H., Cunningham, C.R., Tarling, E.J., Wilks, M.Q., Casero, D., Gray, D.H., Yu, A.K., Wang, E.S.,
1088 Brooks, D.G., Sun, R., Kitchen, S.G., Wu, T.T., Reue, K., Stetson, D.B., Bensinger, S.J., 2015. Limiting
1089 Cholesterol Biosynthetic Flux Spontaneously Engages Type I IFN Signaling. *Cell* 163, 1716-1729.
- 1090 Zaki, A.M., van Boheemen, S., Bestebroer, T.M., Osterhaus, A.D., Fouchier, R.A., 2012. Isolation of a
1091 novel coronavirus from a man with pneumonia in Saudi Arabia. *N Engl J Med* 367, 1814-1820.
- 1092 Zhao, G., Du, L., Ma, C., Li, Y., Li, L., Poon, V.K., Wang, L., Yu, F., Zheng, B.J., Jiang, S., Zhou, Y., 2013. A
1093 safe and convenient pseudovirus-based inhibition assay to detect neutralizing antibodies and screen
1094 for viral entry inhibitors against the novel human coronavirus MERS-CoV. *Virology* 453, 266.
- 1095 Zhou, N., Pan, T., Zhang, J., Li, Q., Zhang, X., Bai, C., Huang, F., Peng, T., Zhang, J., Liu, C., Tao, L.,
1096 Zhang, H., 2016. Glycopeptide Antibiotics Potently Inhibit Cathepsin L in the Late
1097 Endosome/Lysosome and Block the Entry of Ebola Virus, Middle East Respiratory Syndrome
1098 Coronavirus (MERS-CoV), and Severe Acute Respiratory Syndrome Coronavirus (SARS-CoV). *J Biol
1099 Chem* 291, 9218-9232.
- 1100 Zu, S., Deng, Y.Q., Zhou, C., Li, J., Li, L., Chen, Q., Li, X.F., Zhao, H., Gold, S., He, J., Li, X., Zhang, C.,
1101 Yang, H., Cheng, G., Qin, C.F., 2020. 25-Hydroxycholesterol is a potent SARS-CoV-2 inhibitor. *Cell Res*
1102 30, 1043-1045.
- 1103
1104
1105
1106

Declaration of interests

The authors declare that they have no known competing financial interests or personal relationships that could have appeared to influence the work reported in this paper.

The authors declare the following financial interests/personal relationships which may be considered as potential competing interests:

On behalf of all authors,

***I, Wonsik Lee (corresponding authors and lead contact)
confirm that the authors declare no competing interests***

2022, October 20